

## Supplemental Material

### Morpholine catalyzed synthesis of novel 4*H*-chromene linked pyrazole - 1,2,3-triazole hybrids, screening for anticancer and antimicrobial effects

Kishan Chevula,<sup>a</sup> Nagesh Patnam<sup>a</sup>, Prasad Chennamsetti<sup>a</sup>, Vishnu Thumma,<sup>b</sup> Vinutha Kuchana,<sup>c</sup> and Vijjulatha Manga<sup>a\*</sup>

<sup>a</sup>Department of Chemistry, Osmania University, Hyderabad – 500007, Telangana, India

<sup>b</sup>Department of Sciences and Humanities, Matrusri Engineering College, Hyderabad – 500059, Telangana, India

<sup>c</sup>Department of Pharmaceutical Quality Assurance, Sarojini Naidu Vanita Pharmacy Maha Vidyalaya, Hyderabad – 500007, Telangana, India

Email: [vijjulathamanga@gmail.com](mailto:vijjulathamanga@gmail.com)

### Table of Contents

Biological assay procedures and molecular docking study results.....	S2
<sup>1</sup> H and <sup>13</sup> C NMR spectra .....	S9

### MTT assay

The Anticancer activity of the compounds was determined using MTT assay.<sup>1,2</sup>  $1 \times 10^4$  cells/well were seeded in 100  $\mu$ l Dulbecco's Modified Eagle Medium, supplemented with 10% FBS in each well of 96-well microculture plates and incubated for 24 h at 37°C in a CO<sub>2</sub> incubator. After 24 h of incubation, all the synthesized compounds were added to the cells and incubated for 48 h. After 48 h of drug treatment, 10  $\mu$ l MTT (3-(4, 5-dimethylthiazol-2-yl)- 2,5-diphenyl tetrazolium bromide) (5 mg/mL) was added to each well and the plates were further incubated for 4 h. Then the supernatant from each well was carefully removed, formazan crystals were dissolved in 100  $\mu$ l of DMSO and absorbance at 570 nm wavelength was recorded.

### Agar disc diffusion method

The compounds were weighed, dissolved in DMSO to a final concentration of 1mg/ml, and stored. All synthesized compounds were tested for antibacterial and antifungal activity against four pathogenic bacteria (two Gram-positive and two Gram-negative) and two pathogenic fungi using the agar disc diffusion technique. *Staphylococcus aureus*, *Escherichia coli*, *Pseudomonas aeruginosa*, *Bacillus cereus*, and the fungi *Aspergillus Niger* and *Candida albicans* were selected due to their medical and pharmacological importance and were used to assess antimicrobial activity. The bacterial and fungal stock cultures were cultivated for 24 hours at 37°C on nutritious broth (Lauria bertani broth) and potato dextrose agar (PDA) medium, respectively, and then stored in the refrigerator. Bacterial cultures were thoroughly dispersed on LB agar plates, while fungal cultures were evenly spread on PDA plates. The compounds were then placed on filter paper discs and cultured at 37°C for 24 hours for bacteria and 48 hours at 28°C for fungal strains. Mm is the zone of inhibition. Standard substances ciprofloxacin (100  $\mu$ g/ml) and fluconazole (100  $\mu$ g/ml) were used as controls for bacterial and fungal strains, respectively.

### MIC determination

The Minimal inhibitory concentration of all synthesized compounds against bacterial and fungal strains was determined using a 96 well-plate micro-dilution technique. All synthesized compounds were diluted to different concentrations (5 – 100  $\mu$ g/ml) and added to 100  $\mu$ l of bacterial and fungal cultures in a 96 well plate, where they were cultured overnight at 37°C for bacteria and 28°C for fungal strains. Later, the growth of bacterial and fungal strains was observed at 600 nm and 620 nm, respectively. The minimum inhibitory concentration (MIC) of each substance was determined to be the lowest concentration that inhibited microbial growth.

### Molecular docking procedure

Autodock Vina integrated PyRx tool was employed for docking simulations. The crystal structure of target proteins were retrieved from Protein Data Bank ([www.rcsb.org](http://www.rcsb.org)). Initially, water molecules and heteroatoms of protein were removed and added polar hydrogens. The

ligands were sketched using ChemDraw Professional 16.0 in MDL file (.mol) format. Minimized the energies of all ligands after loading into PyRx and converted to PDBQT file format. The 3D grid box was configured as shown in Table 6, docking simulations were performed after assigning the exhaustiveness value of 8. The docking result were visualized using Pymol and Biovia Discovery Studio Visualizer.

**Table 6** Grid box configuration

PDB ID	Dimensions
2J6M	center_x = -53.0844483254, center_y = -1.37854954138, center_z = -18.0646785138, size_x = 17.4911216889, size_y = 17.4440509575 and size_z = 27.0353935141
2XCT	center_x = 6.13473955324, center_y = 51.5379078718, center_z = 76.2996508168, size_x = 10.3153368175, size_y = 15.2043696148 and size_z = 19.6777984709
4WMZ	center_x = 29.1083397384, center_y = 8.51285114595, center_z = 11.1695252666, size_x = 13.8981770078, size_y = 15.4693022919 and size_z = 15.3425708068

### Molecular docking against EGFR kinase

To get an insight on the binding interactions, computational screening performed against the crystal structure of Epidermal Growth Factor Receptor (EGFR) (PDB ID: 2J6M)<sup>3</sup> using most potent ligand **4i**. EGFR, a transmembrane glycoprotein, belongs to the ERBB receptor tyrosine kinase superfamily. EGFR interacts with its specific ligand EGF, resulting in tyrosine phosphorylation and receptor dimerization with other family members, which promotes uncontrolled proliferation.<sup>4-6</sup> The docking results were confirmed by re-docking the co-crystallized ligand AEE788 into the EGFR cavity. The AEE788 exhibited RMSD values of 1.13 Å and demonstrated a binding affinity of -9.2 kcal/mol for EGFR. The docking score of ligand **4i** was reported to be -10.2 kcal/mol, which had displayed three key interactions with amino acid sites Met793(2) and Arg841 of EGFR, one of the binding interaction distances with Met793 was found to be 2.32 Å (strong) and another one with 2.49 Å (moderate). The bond distance with Arg841 was seen to be 3.30 Å (weak). Additionally, hydrophobic interactions were displayed with Phe723, Ala743, Lys745, Leu788, Thr790, Arg841, Leu844 and Asp855 of EGFR (Figure 2). Among these, a valuable  $\pi$ - $\pi$  stacked interaction with Phe723 and a  $\pi$ -anion interaction with Asp855 appeared. The co-crystallized ligand AEE788 had displayed two H-bond interactions with Gln791 and Met793, and hydrophobic interactions with Leu718, Val726, Val743, Lys745, Leu788, Thr790, Asp800 and Leu844 of EGFR (Figure 3). The dock pose image (Figure 4) of ligand **4i** along with AEE788 in cavity of EGFR showed their fit, essential for binding.

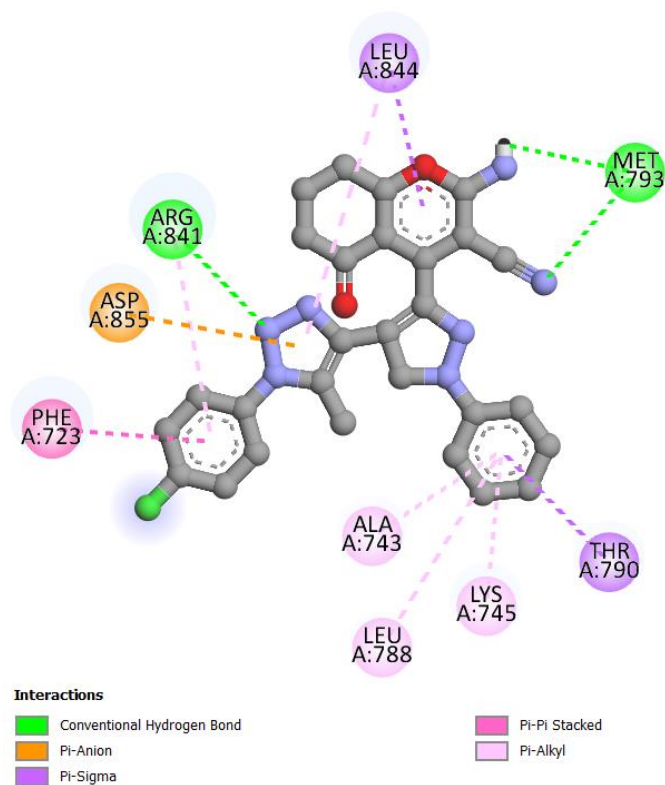


**Figure 2.** Binding interactions of ligand **4i** against EGFR.

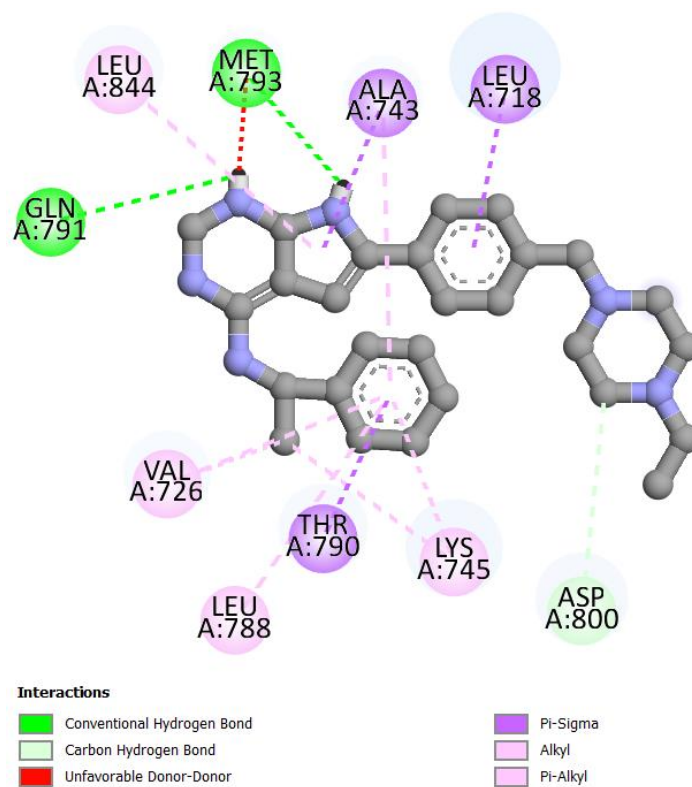


**Figure 3.** Binding interactions of AEE788 against EGFR.

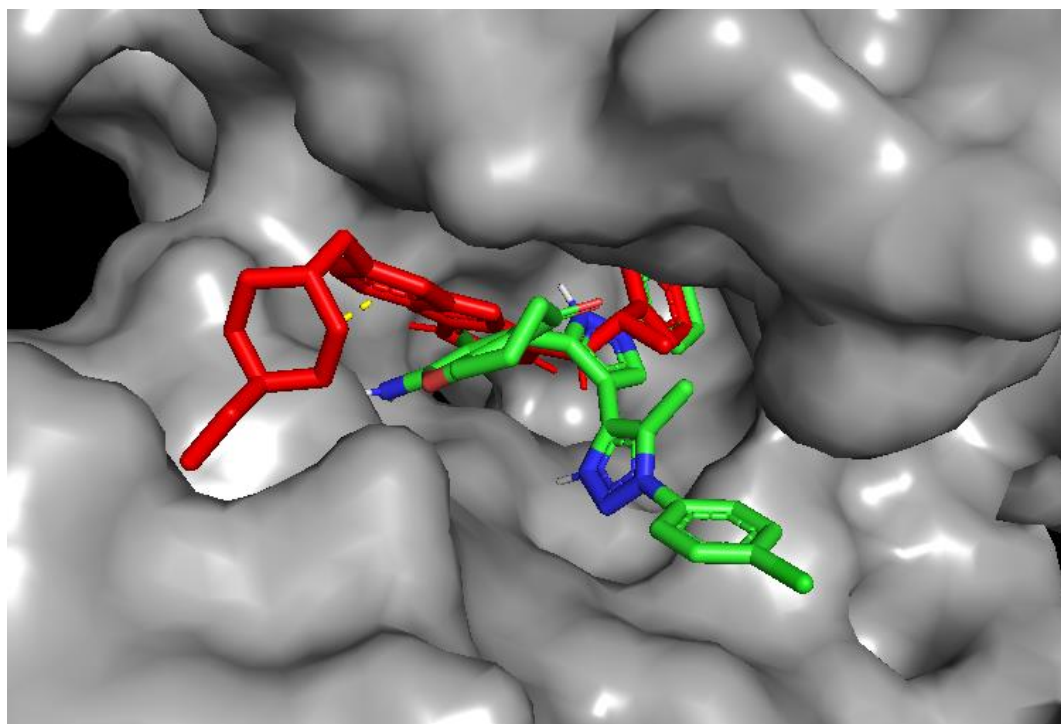


**Figure 4.** Dock pose image of ligand **4i** (green) and AEE788 (red) in cavity of EGFR.

#### Molecular docking against DNA gyrase and Lanosterol 14-alpha demethylase

To understand the binding interactions of synthesized compounds and molecular target, performed *In silico* screening against crystal structure of DNA gyrase subunit B (PDB ID: 2XCT)<sup>7</sup> and Lanosterol 14-alpha demethylase (PDB ID: 4WMZ)<sup>8</sup> which are the targets of Ciprofloxacin and Fluconazole respectively. One of the best active ligand **4i** chosen for docking study, validated the docking program by re-docking co-crystallized ligands ciprofloxacin (RMSD = 1.15 Å) and fluconazole (RMSD = 1.04 Å) against respective proteins. The binding score of ligand **4i** was found to be encouraging with -9.1 kcal/mol against DNA gyrase and -10.0 kcal/mol against Lanosterol 14-alpha demethylase. Whereas Ciprofloxacin and Fluconazole scored binding affinity value of -7.0 kcal/mol and -7.4 kcal/mol.

The ligand **4i** envisioned two  $\pi$ -anion interactions with Lys460 and Asp510, and a  $\pi$ -cation interaction with Asp512 of DNA gyrase (Figure 5). Checking with reference ligand ciprofloxacin, displayed two H-bond interactions with Asp510 and a  $\pi$ - $\pi$  T shaped interaction with His1081 of DNA gyrase (Figure 6). Some of the hydrophobic interactions of ciprofloxacin coinciding with the ligand **4i** interactions. The dock pose image (Figure 7) of ligand **4i** and ciprofloxacin revealed that these molecules best fit into the active site pocket of DNA gyrase. Further, the docking score of ligand **4i** was greater against Lanosterol 14-alpha demethylase with promising binding interactions (Figure 8). These interactions were of very interesting, it showed a key interaction with Tyr140 of Lanosterol 14-alpha demethylase, the bond distance was reported to be 1.74 Å proving strong interaction. Additionally, a  $\pi$ -sulfur interaction with Cys470, and other hydrophobic interactions with Ile139, Lys151, Val154, Leu212, Leu307, Val311, Leu383, Ile471 and Phe475 of Lanosterol 14-alpha demethylase. The reference ligand

fluconazole showed one H-bond interaction with Gly310, a halogen bond interaction with Gln150, and other hydrophobic interactions with Ile139, Lys151 and Val311 of Lanosterol 14-alpha demethylase (Figure 9). In this case also some of the interactions of ligand **4i** coincided with the interaction of fluconazole. It could be also understood from the dock pose image (Figure 10) of ligand **4i** and fluconazole in cavity of Lanosterol 14-alpha demethylase. In comparison ligand **4i** had shown more binding affinity towards Lanosterol 14-alpha demethylase compared to DNA gyrase.

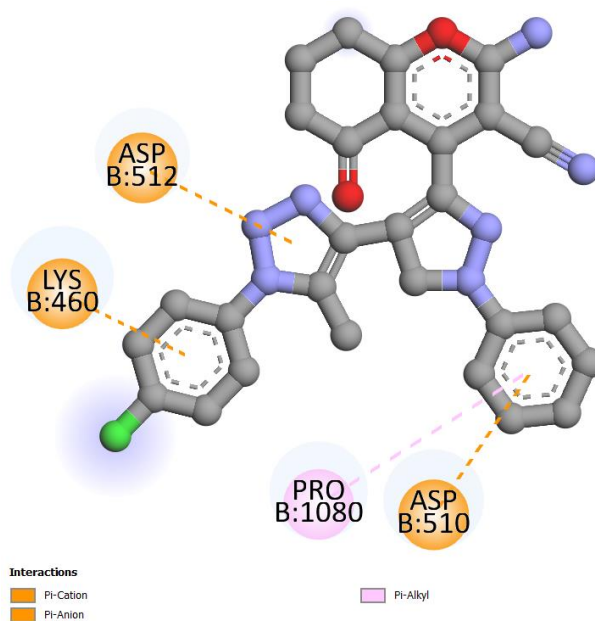


**Figure 5.** Binding interaction of ligand **4i** against DNA gyrase.

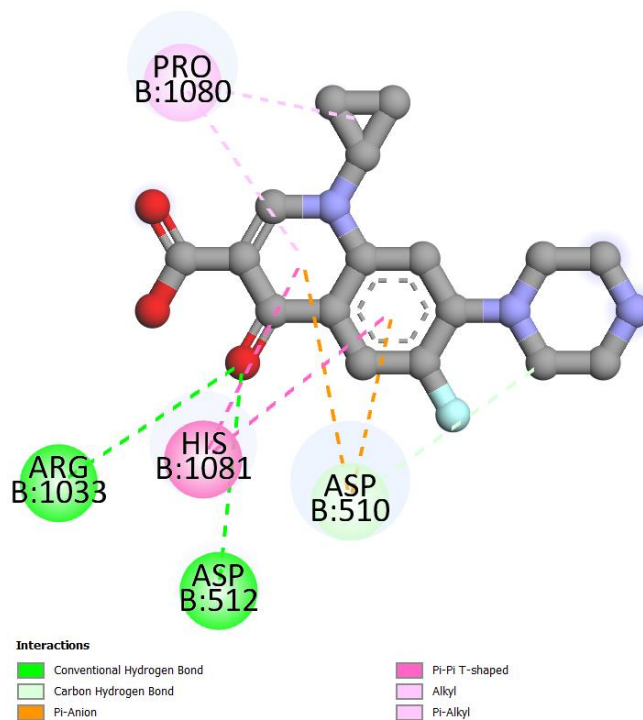


**Figure 6.** Binding interactions of ciprofloxacin against DNA gyrase.

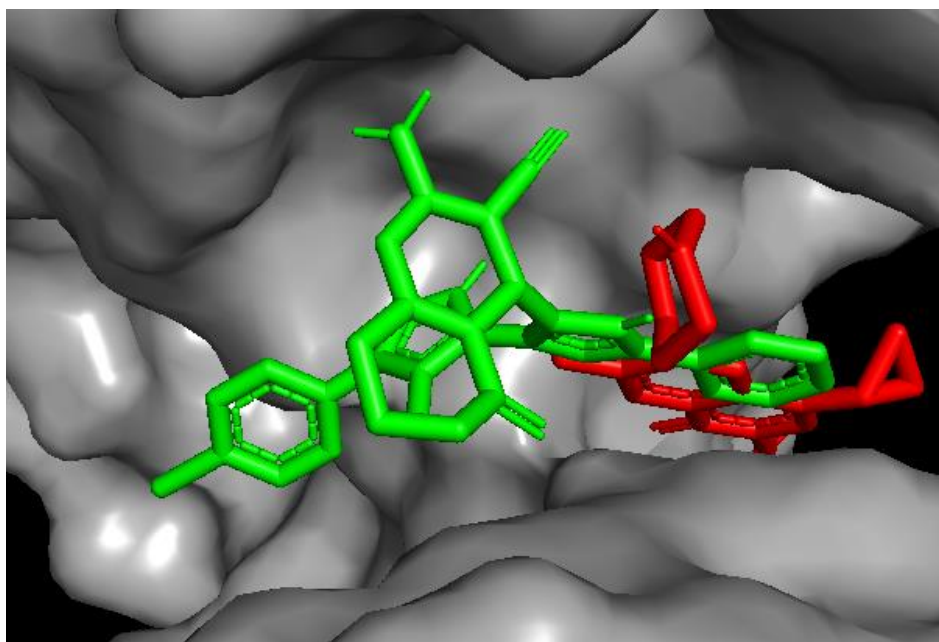


**Figure 7.** Dock pose of ligand **4i** (green) and ciprofloxacin (red) in active site pocket of DNA gyrase

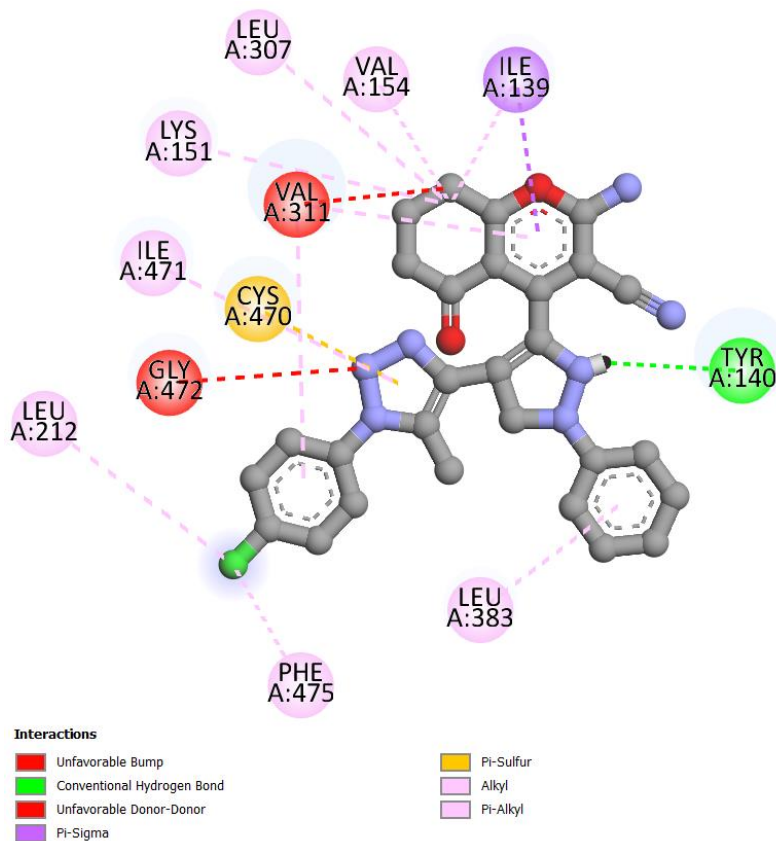


**Figure 8.** Binding interactions of ligand **4i** against Lanosterol 14-alpha demethylase.

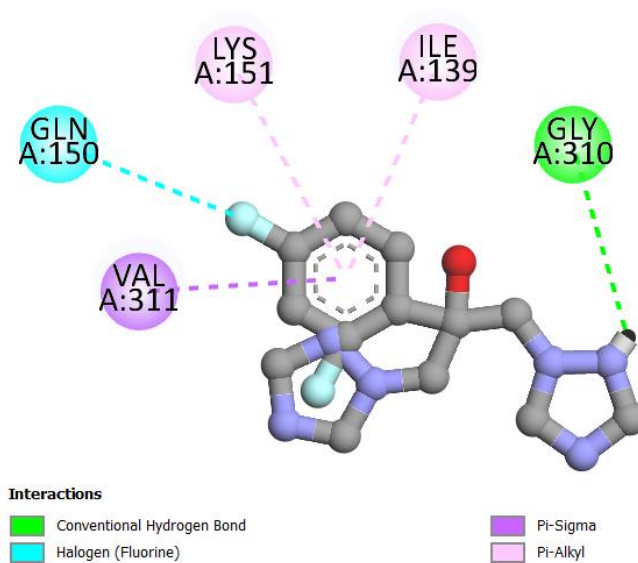


**Figure 9.** Binding interactions of fluconazole against Lanosterol 14-alpha demethylase.

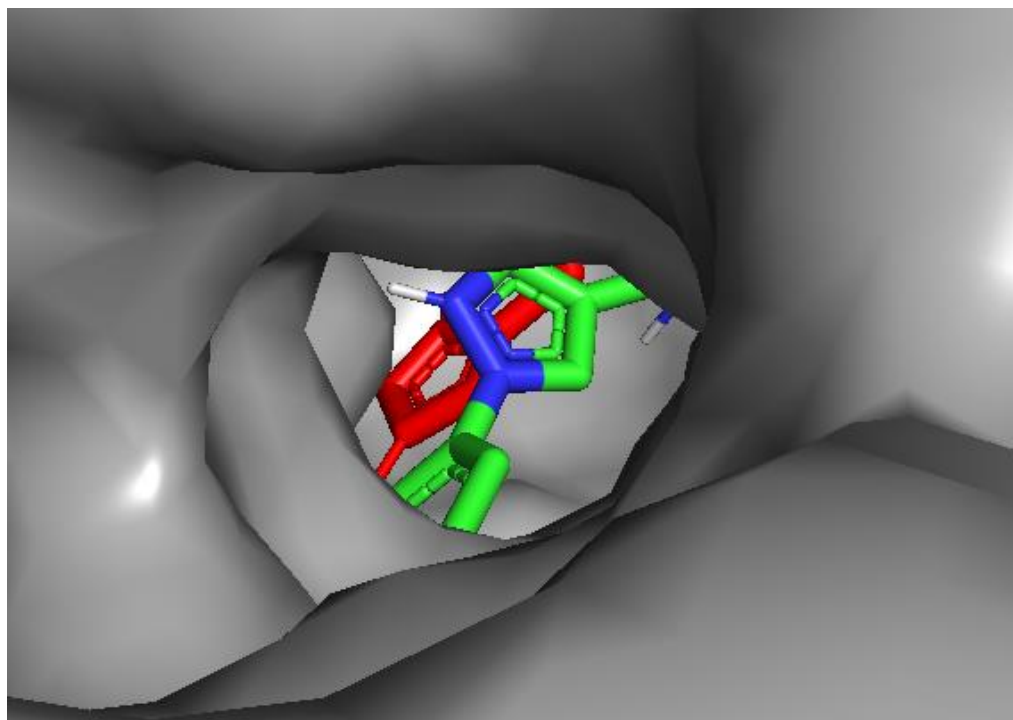
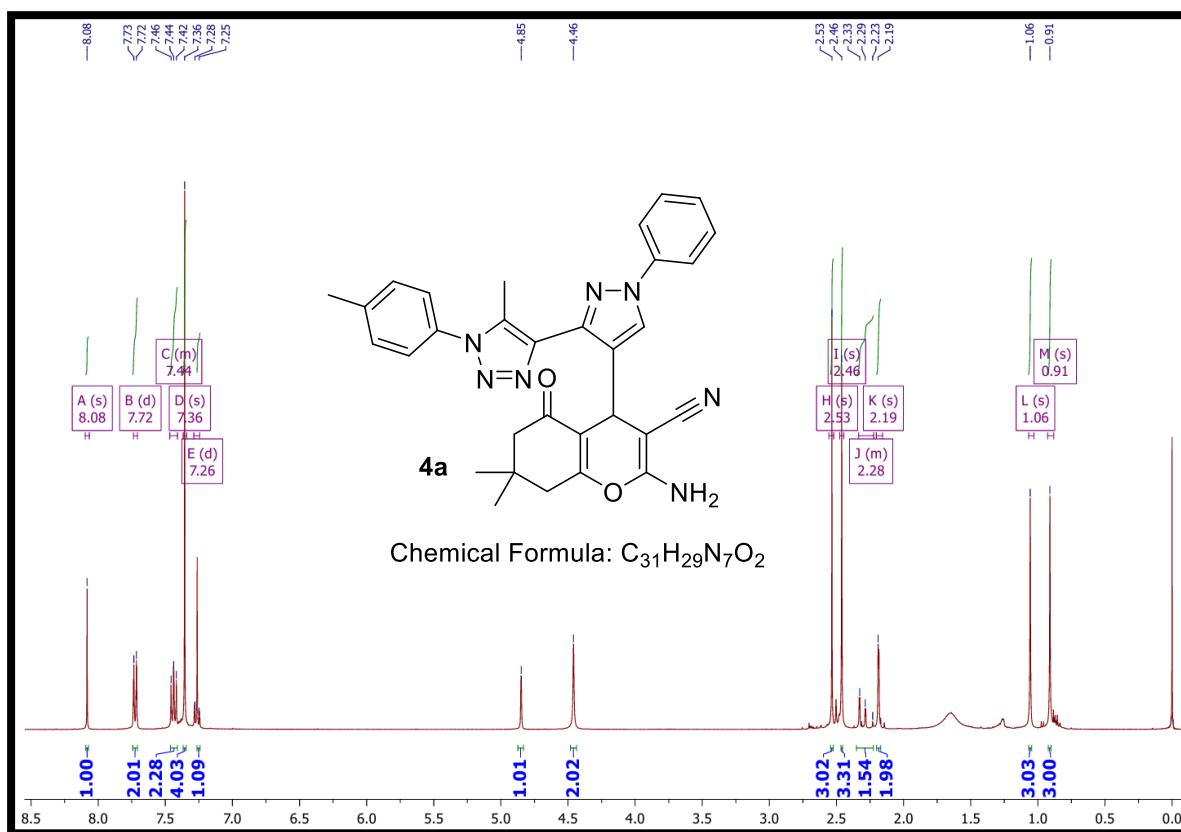
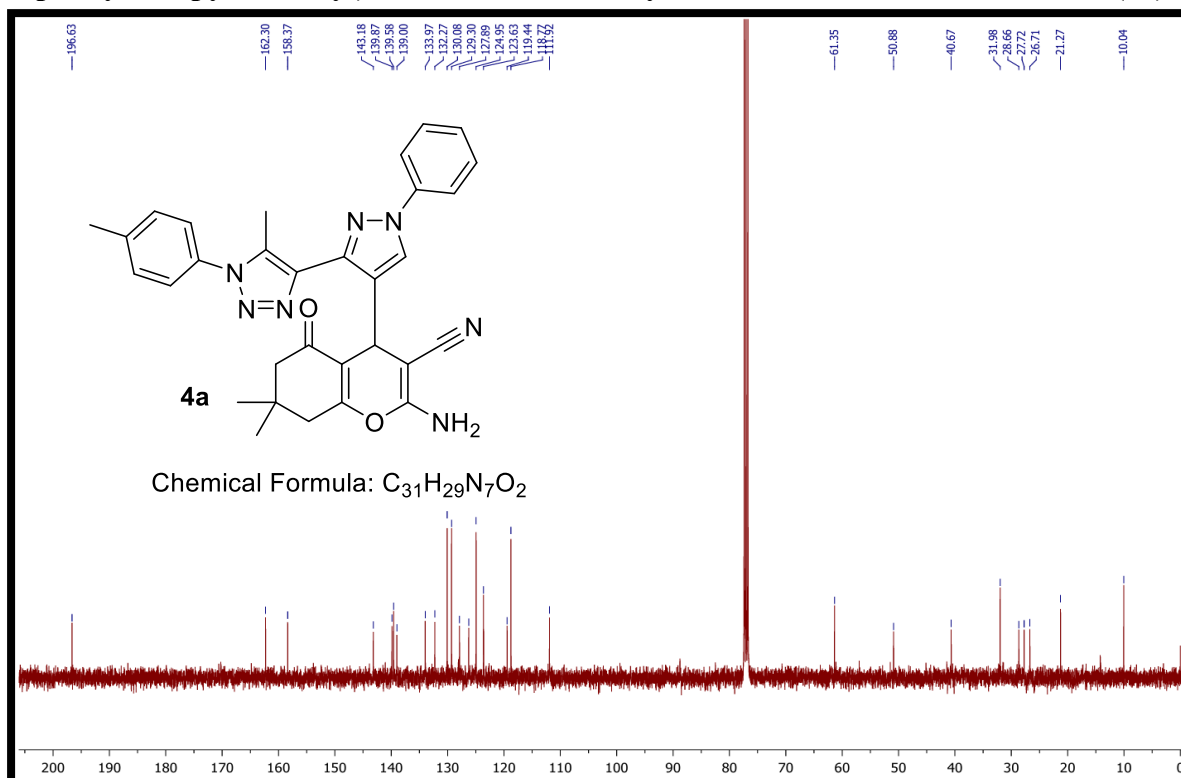


**Figure 10.** Dock pose image of ligand **4i** (green) and fluconazole (red) in active site pocket of Lanosterol 14-alpha demethylase.

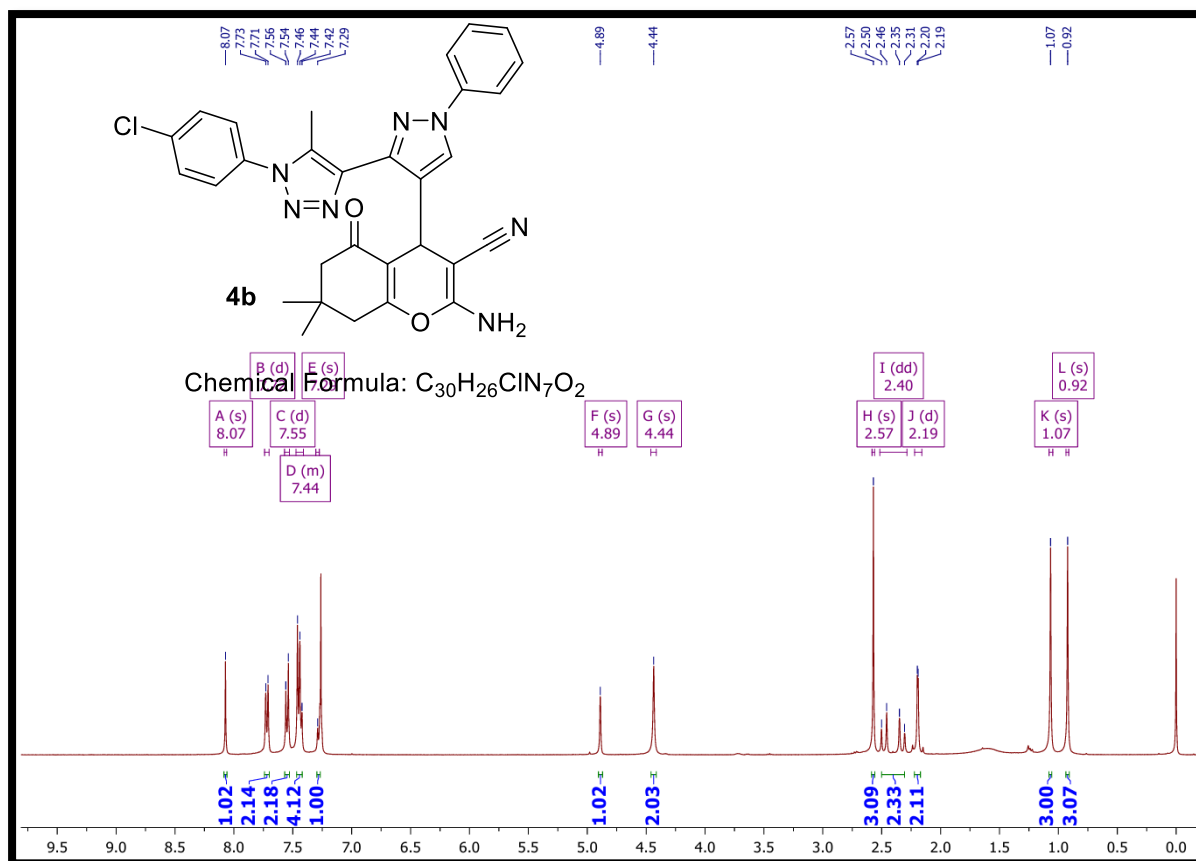
## Spectral Copies



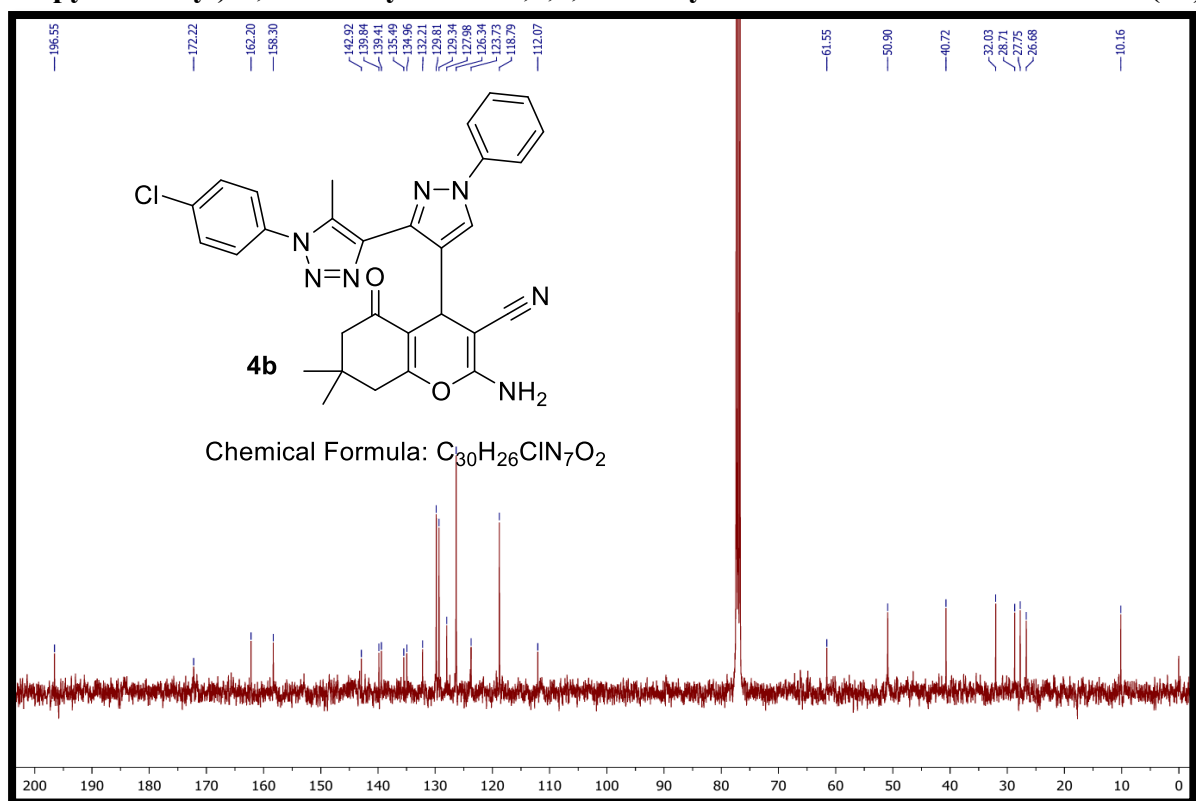
<sup>1</sup>H NMR of 2-amino-7,7-dimethyl-4-(3-(5-methyl-1-(p-tolyl)-1H-1,2,3-triazol-4-yl)-1-phenyl-1H-pyrazol-4-yl)-5-oxo-5,6,7,8-tetrahydro-4H-chromene-3-carbonitrile (4a)



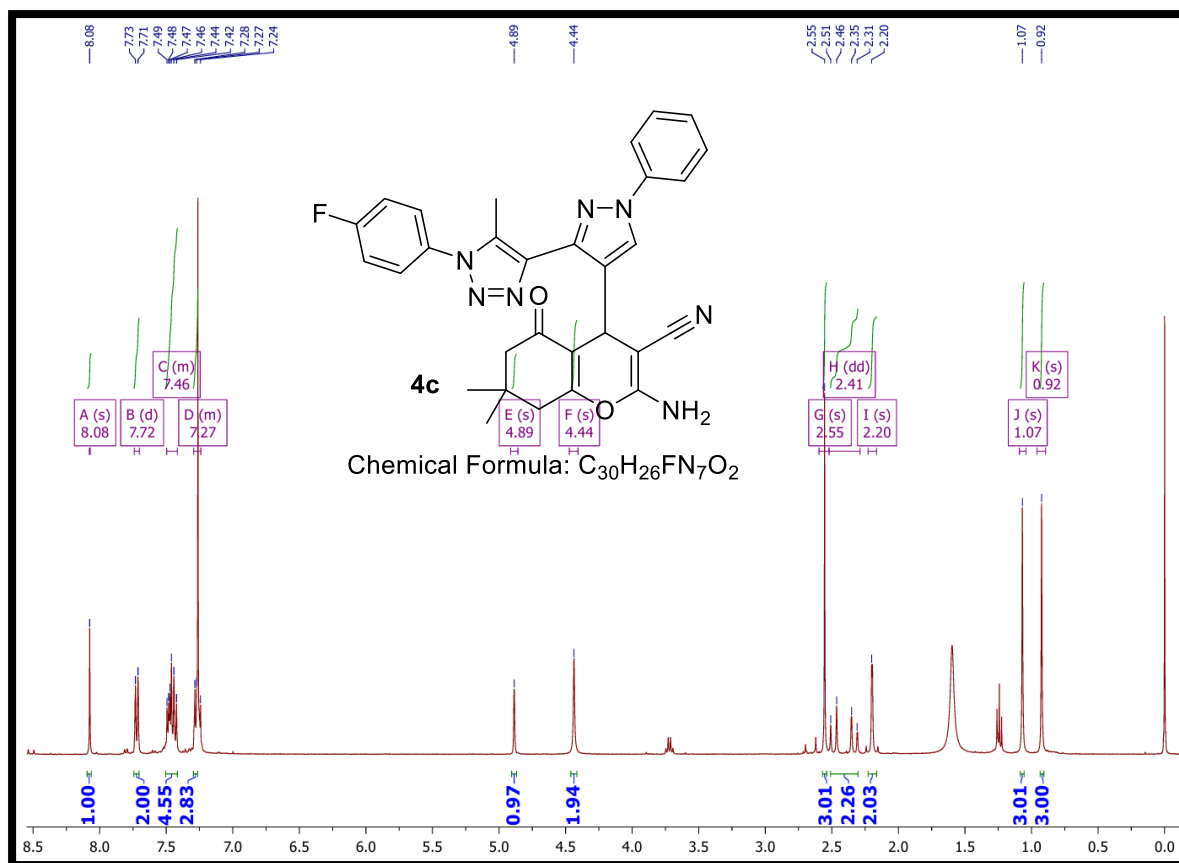
<sup>13</sup>C NMR of 2-amino-7,7-dimethyl-4-(3-(5-methyl-1-(p-tolyl)-1H-1,2,3-triazol-4-yl)-1-phenyl-1H-pyrazol-4-yl)-5-oxo-5,6,7,8-tetrahydro-4H-chromene-3-carbonitrile (4a)



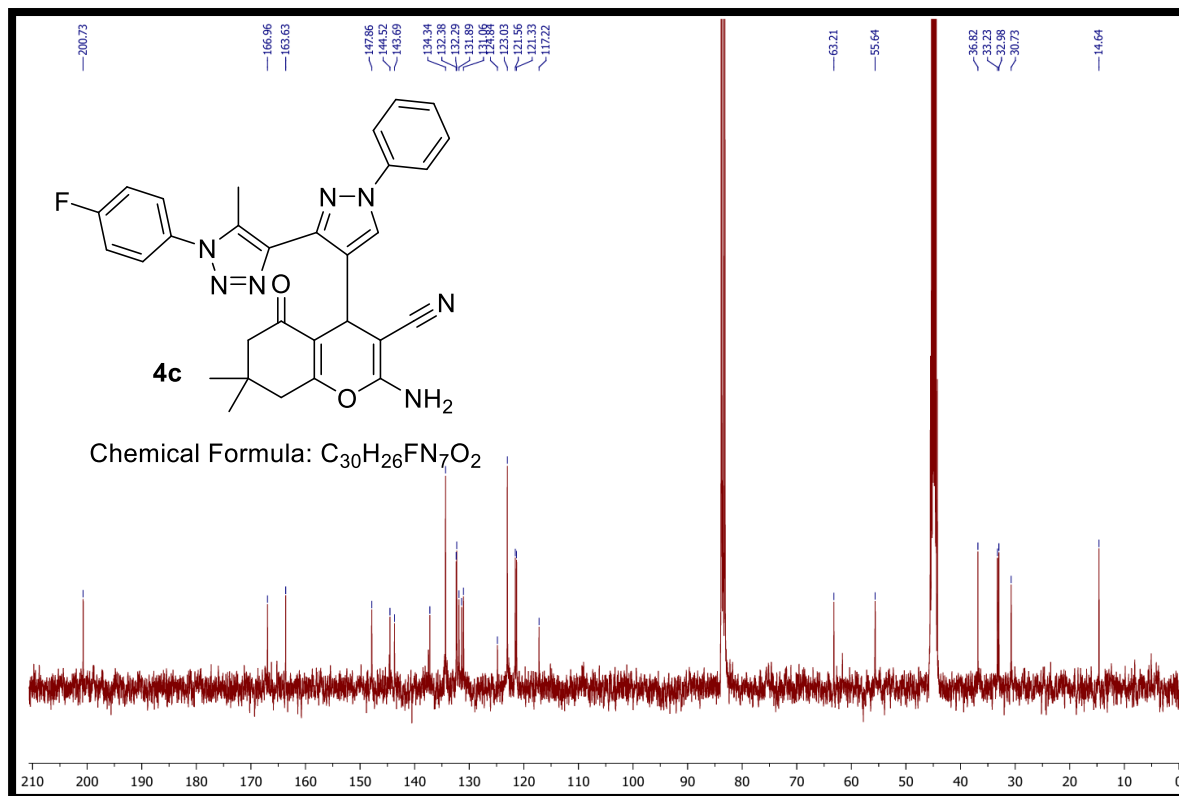
**<sup>1</sup>H NMR** of 2-amino-4-(3-(1-(4-chlorophenyl)-5-methyl-1H-1,2,3-triazol-4-yl)-1-phenyl-1H-pyrazol-4-yl)-7,7-dimethyl-5-oxo-5,6,7,8-tetrahydro-4H-chromene-3-carbonitrile(4b)



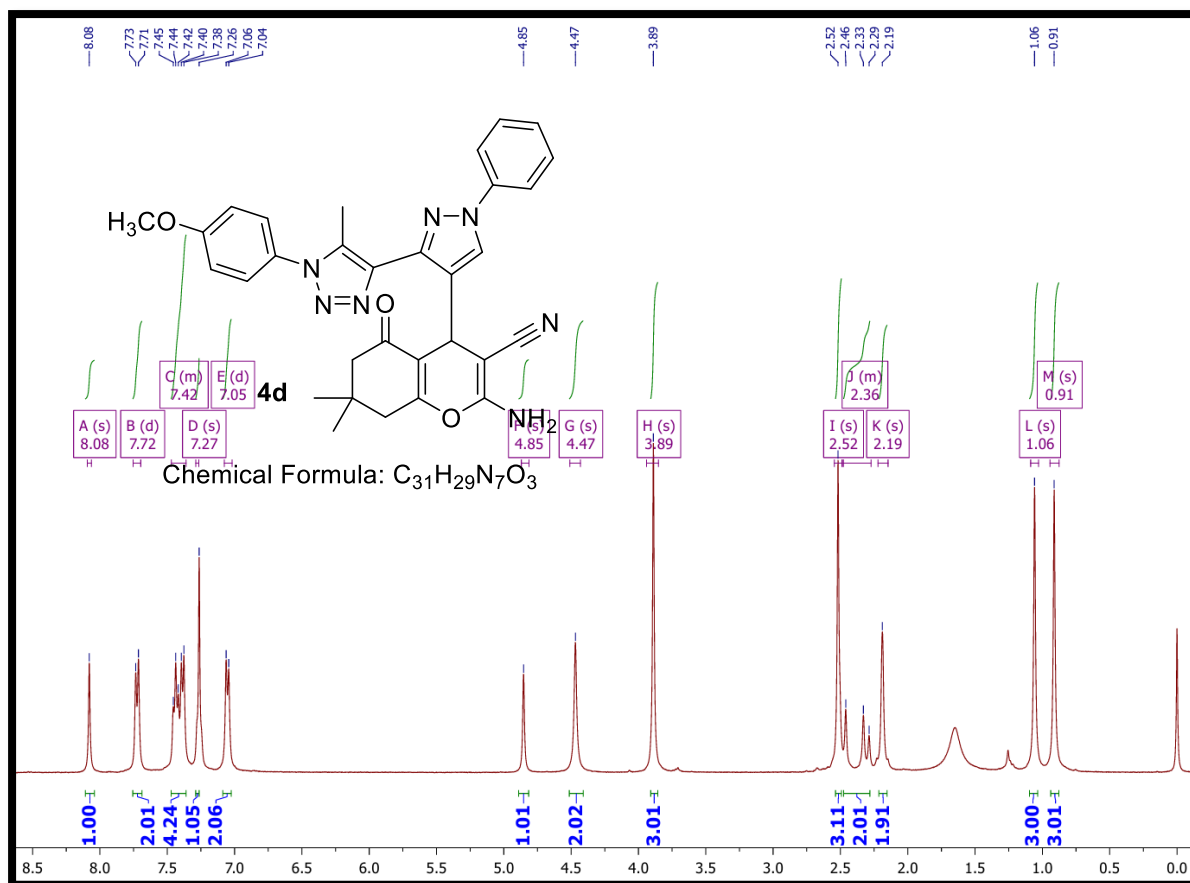
**<sup>13</sup>C NMR** of 2-amino-4-(3-(1-(4-chlorophenyl)-5-methyl-1H-1,2,3-triazol-4-yl)-1-phenyl-1H-pyrazol-4-yl)-7,7-dimethyl-5-oxo-5,6,7,8-tetrahydro-4H-chromene-3-carbonitrile(4b)



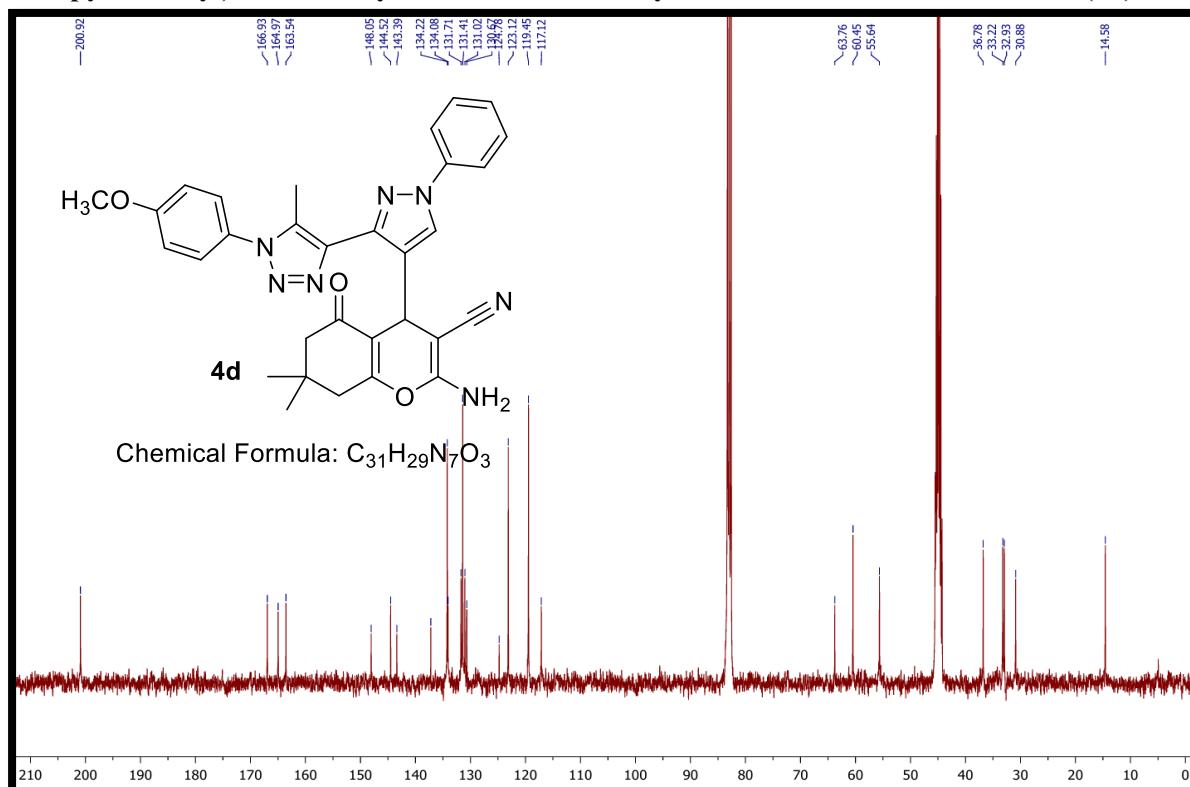
**<sup>1</sup>H NMR** of 2-amino-4-(3-(1-(4-fluorophenyl)-5-methyl-1H-1,2,3-triazol-4-yl)-1-phenyl-1H-pyrazol-4-yl)-7,7-dimethyl-5-oxo-5,6,7,8-tetrahydro-4H-chromene-3-carbonitrile(**4c**)



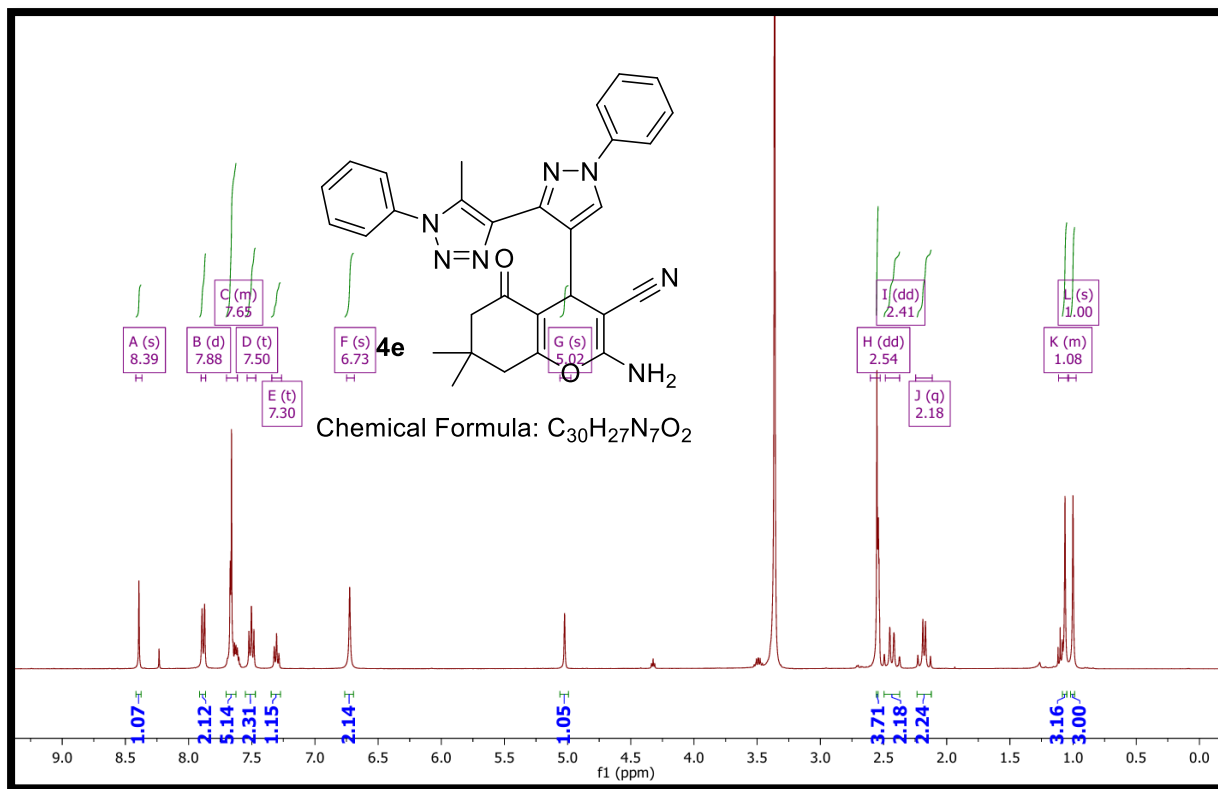
**<sup>13</sup>C NMR** of 2-amino-4-(3-(1-(4-fluorophenyl)-5-methyl-1H-1,2,3-triazol-4-yl)-1-phenyl-1H-pyrazol-4-yl)-7,7-dimethyl-5-oxo-5,6,7,8-tetrahydro-4H-chromene-3-carbonitrile(**4c**)



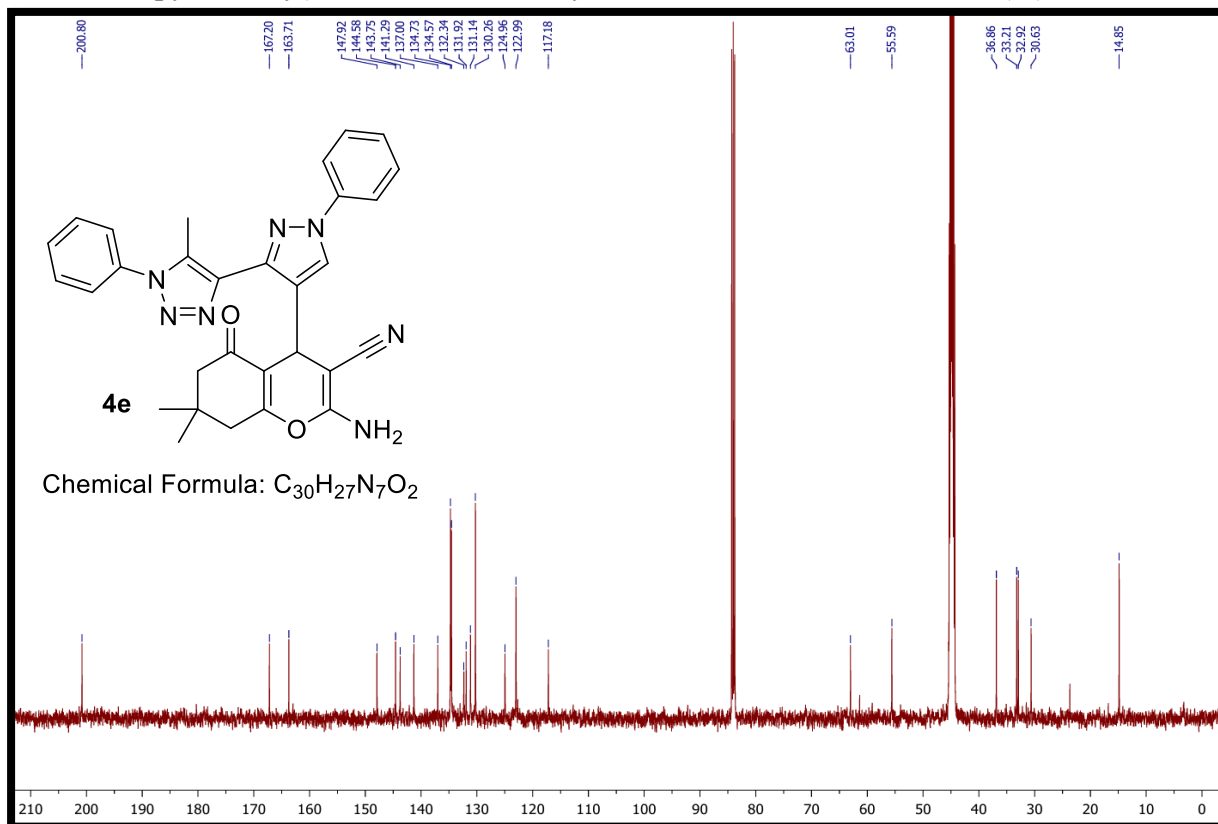
$^1\text{H}$  NMR of 2-amino-4-(3-(1-(4-methoxyphenyl)-5-methyl-1H-1,2,3-triazol-4-yl)-1-phenyl-1H-pyrazol-4-yl)-7,7-dimethyl-5-oxo-5,6,7,8-tetrahydro-4H-chromene-3-carbonitrile (4d)



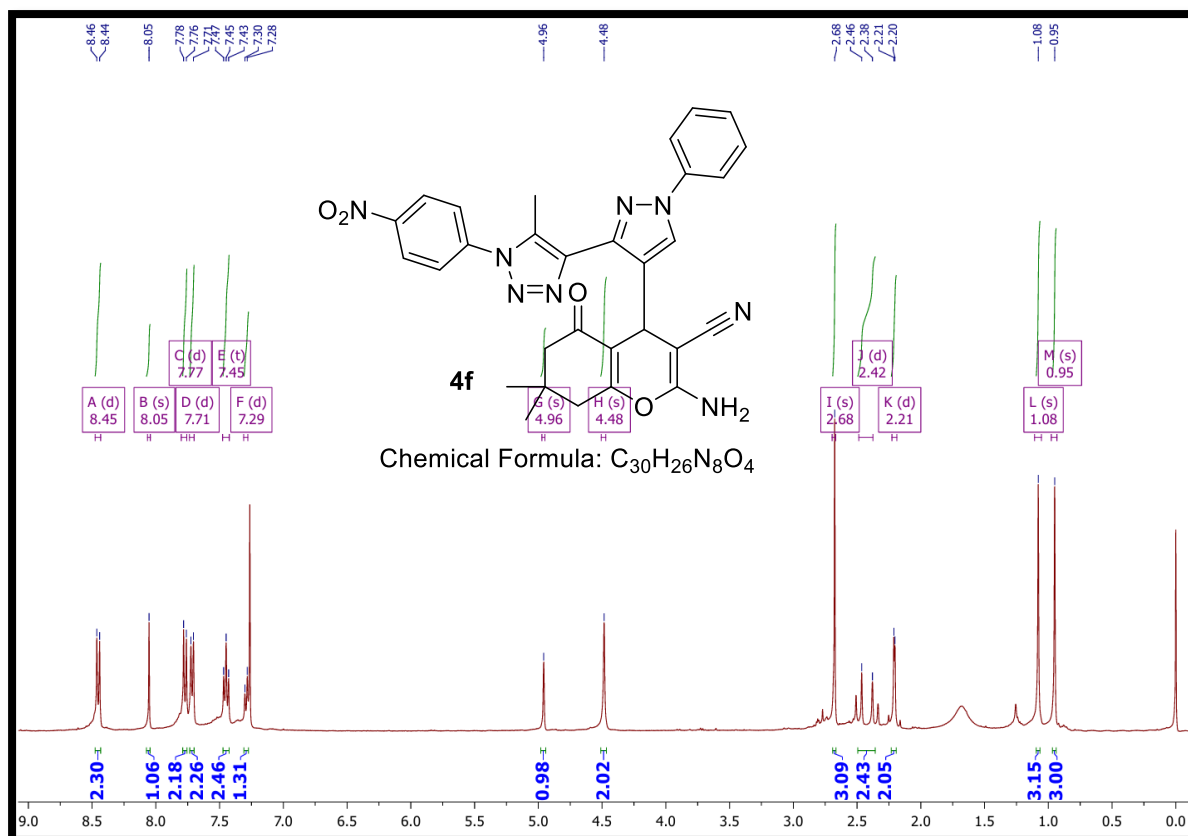
$^{13}\text{C}$  NMR of 2-amino-4-(3-(1-(4-methoxyphenyl)-5-methyl-1H-1,2,3-triazol-4-yl)-1-phenyl-1H-pyrazol-4-yl)-7,7-dimethyl-5-oxo-5,6,7,8-tetrahydro-4H-chromene-3-carbonitrile (4d)



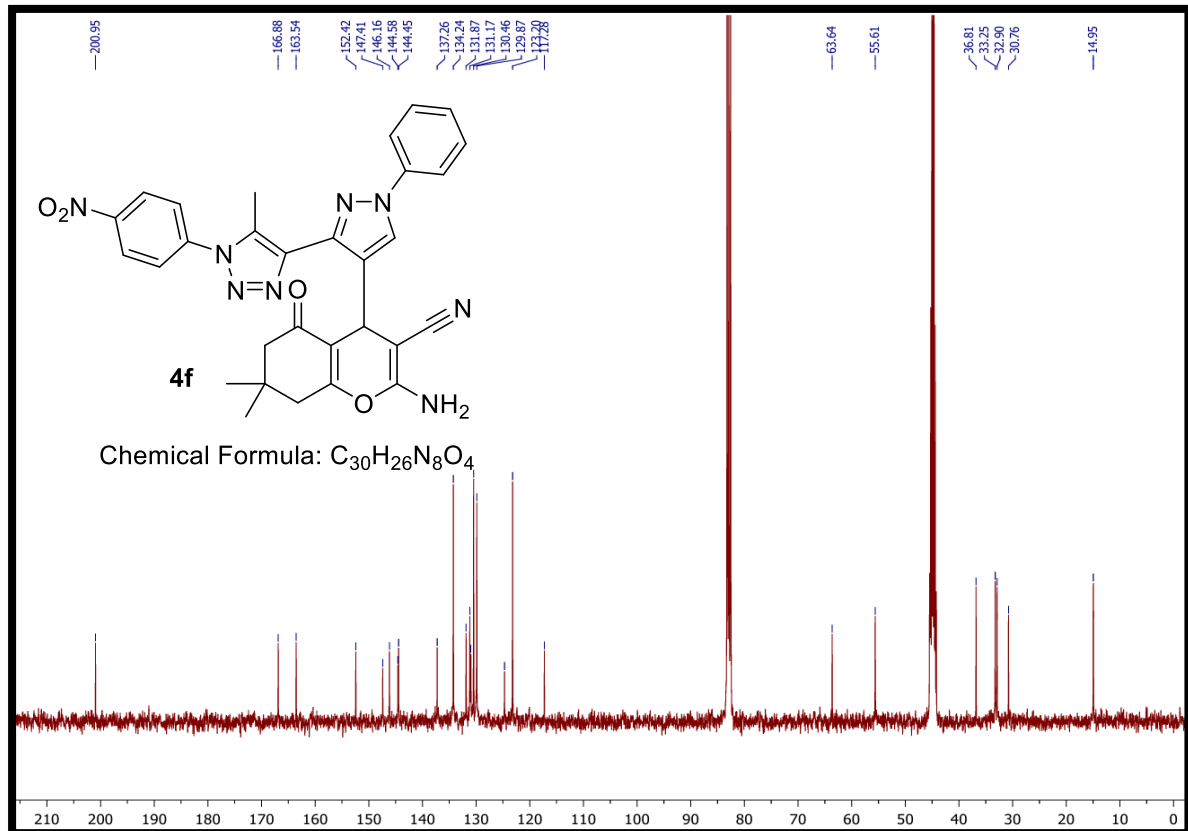
$^1H$  NMR of 2-amino-7,7-dimethyl-4-(3-(5-methyl-1-phenyl-1H-1,2,3-triazol-4-yl)-1-phenyl-1H-pyrazol-4-yl)-5-oxo-5,6,7,8-tetrahydro-4H-chromene-3-carbonitrile (4e)



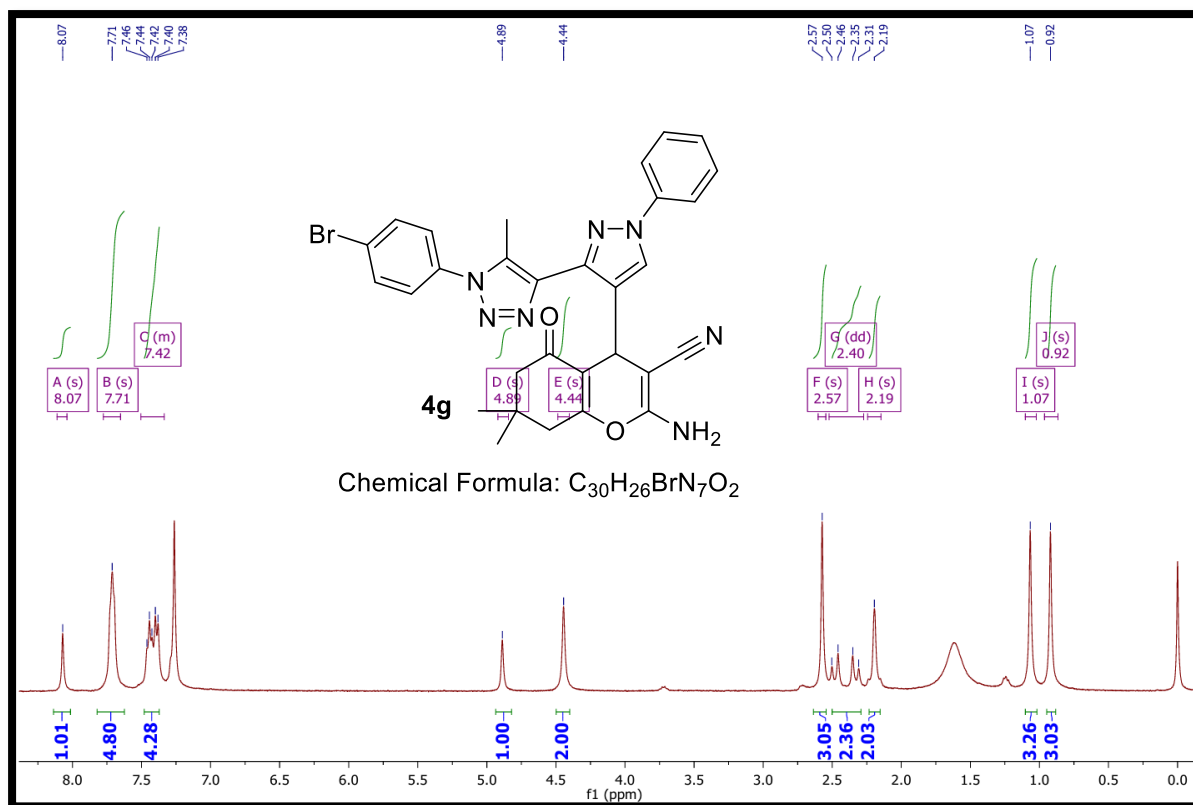
$^{13}C$  NMR of 2-amino-7,7-dimethyl-4-(3-(5-methyl-1-phenyl-1H-1,2,3-triazol-4-yl)-1-phenyl-1H-pyrazol-4-yl)-5-oxo-5,6,7,8-tetrahydro-4H-chromene-3-carbonitrile (4e)



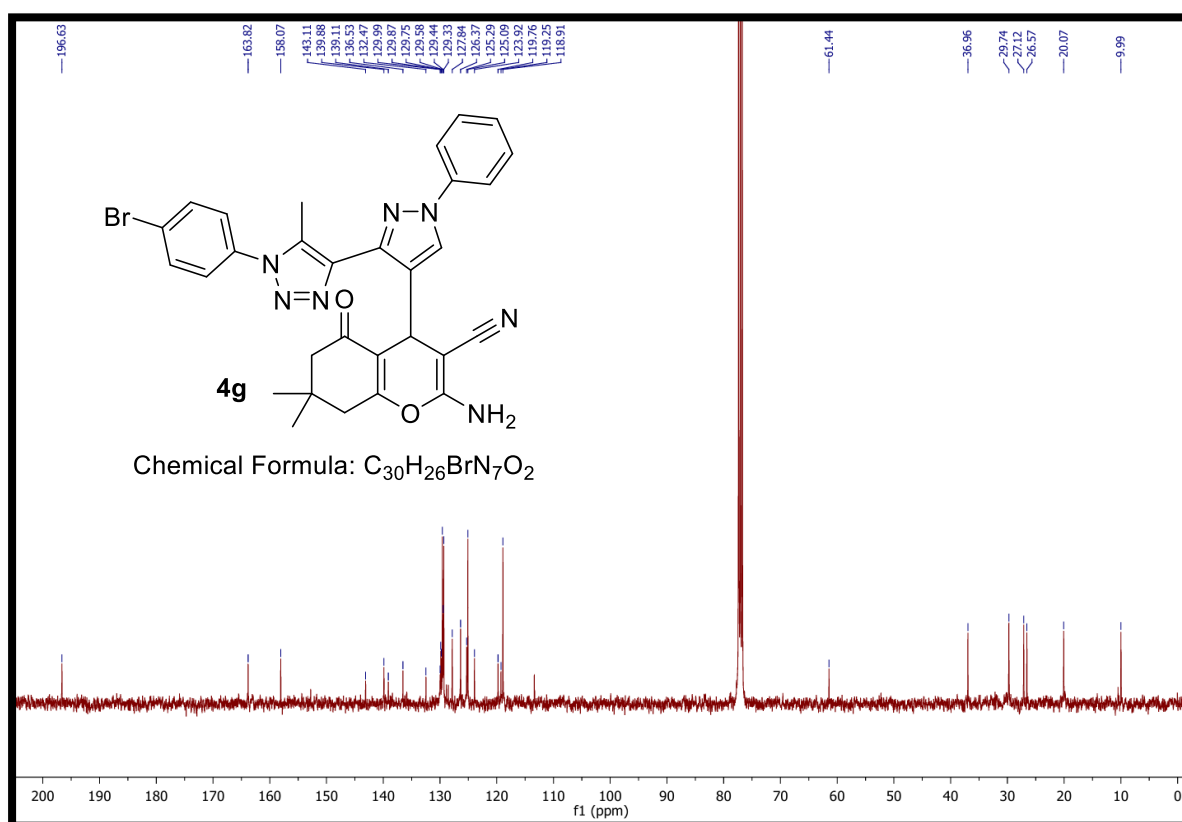
<sup>1</sup>H NMR of 2-amino-7,7-dimethyl-4-(3-(5-methyl-1-(4-nitrophenyl)-1H-1,2,3-triazol-4-yl)-1-phenyl-1H-pyrazol-4-yl)-5-oxo-5,6,7,8-tetrahydro-4H-chromene-3-carbonitrile (**4f**)



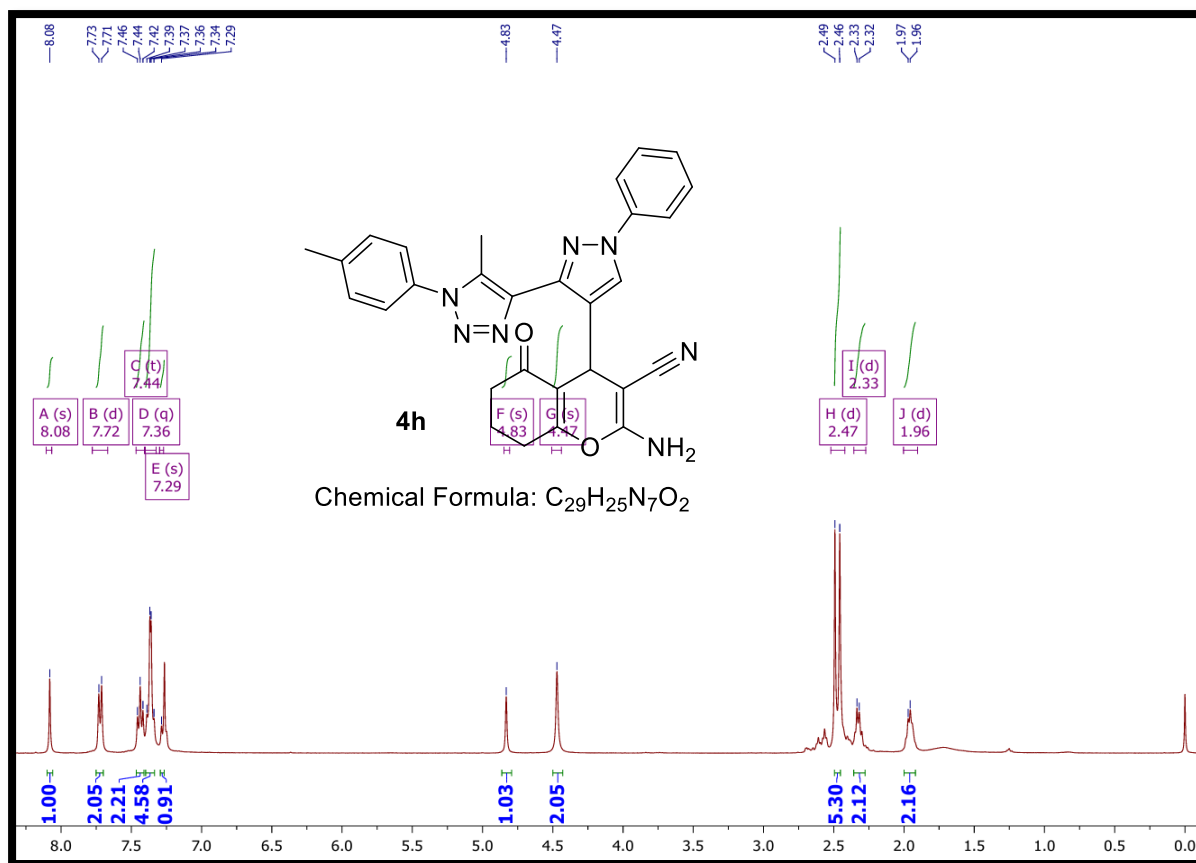
<sup>13</sup>C NMR of 2-amino-7,7-dimethyl-4-(3-(5-methyl-1-(4-nitrophenyl)-1H-1,2,3-triazol-4-yl)-1-phenyl-1H-pyrazol-4-yl)-5-oxo-5,6,7,8-tetrahydro-4H-chromene-3-carbonitrile (**4f**)



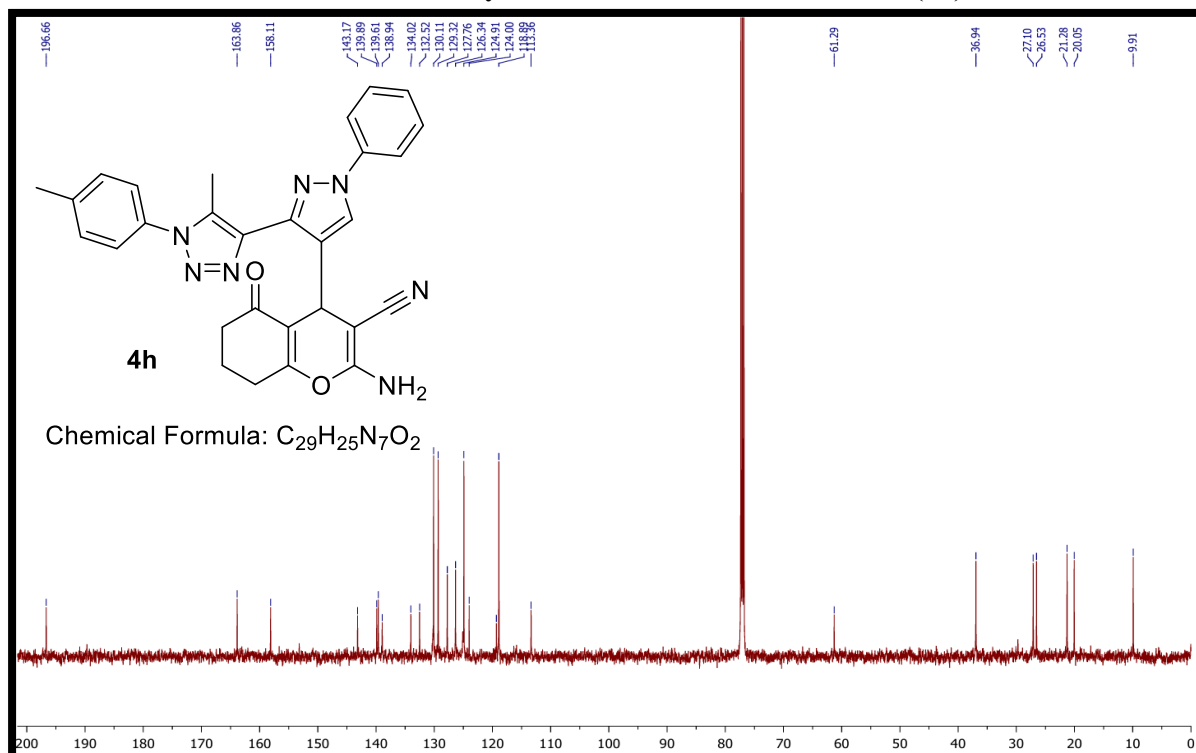
**<sup>1</sup>H NMR** of 2-amino-4-(3-(1-(4-bromophenyl)-5-methyl-1H-1,2,3-triazol-4-yl)-1-phenyl-1H-pyrazol-4-yl)-7,7-dimethyl-5-oxo-5,6,7,8-tetrahydro-4H-chromene-3-carbonitrile(4g)



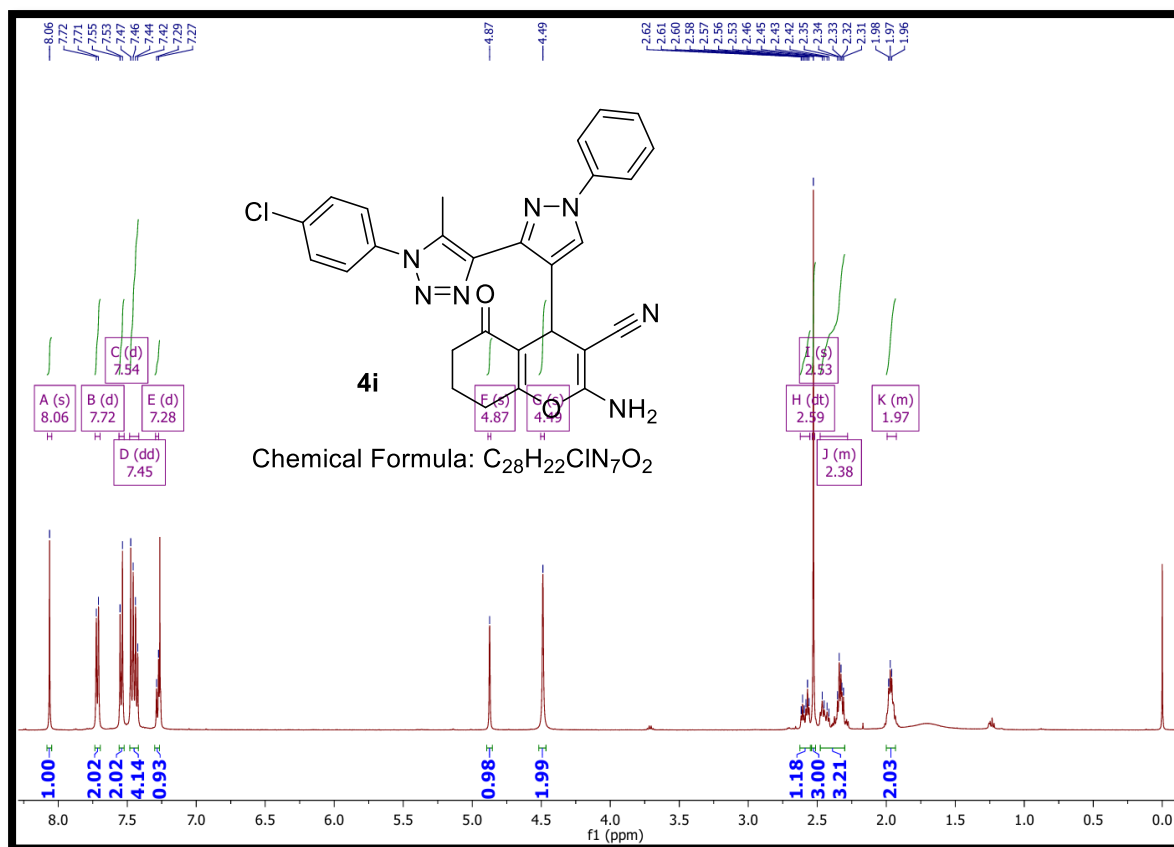
**<sup>13</sup>C NMR** of 2-amino-4-(3-(1-(4-bromophenyl)-5-methyl-1H-1,2,3-triazol-4-yl)-1-phenyl-1H-pyrazol-4-yl)-7,7-dimethyl-5-oxo-5,6,7,8-tetrahydro-4H-chromene-3-carbonitrile(4g)



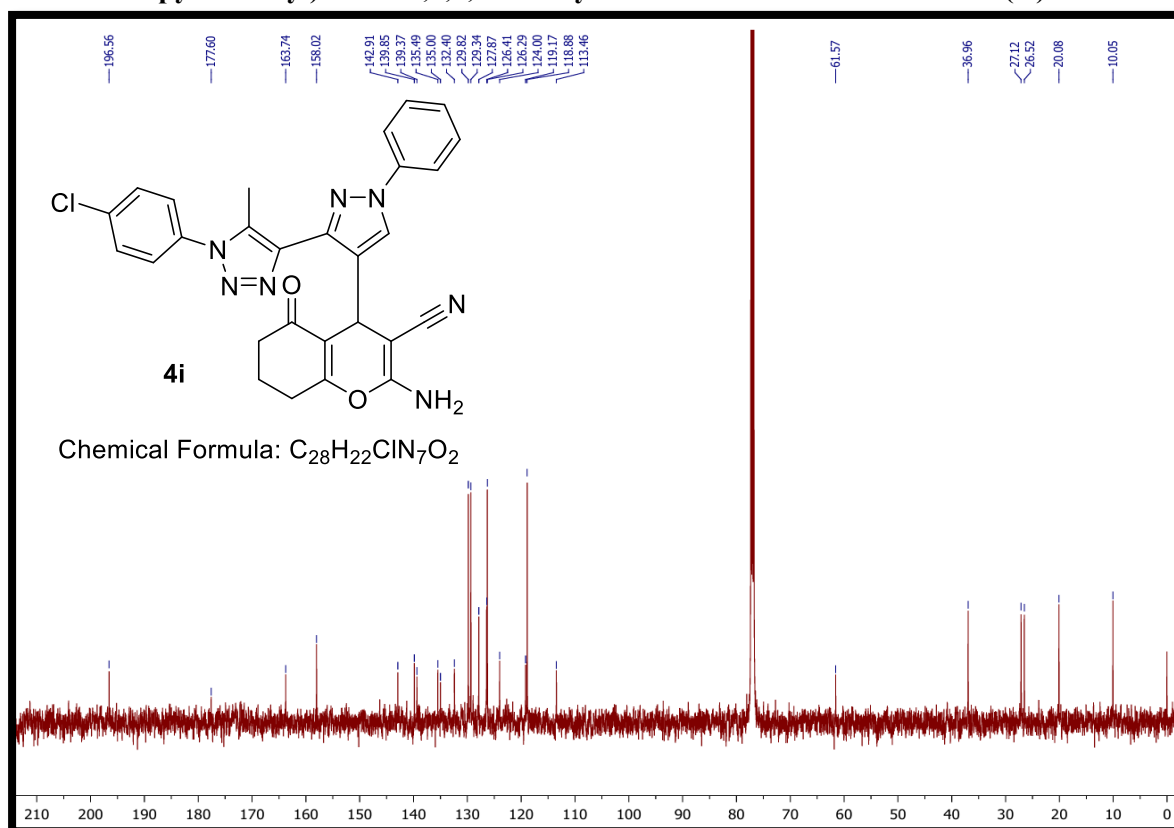
<sup>1</sup>H NMR of 2-amino-4-(3-(5-methyl-1-(p-tolyl)-1H-1,2,3-triazol-4-yl)-1-phenyl-1H-pyrazol-4-yl)-5-oxo-5,6,7,8-tetrahydro-4H-chromene-3-carbonitrile (4h)



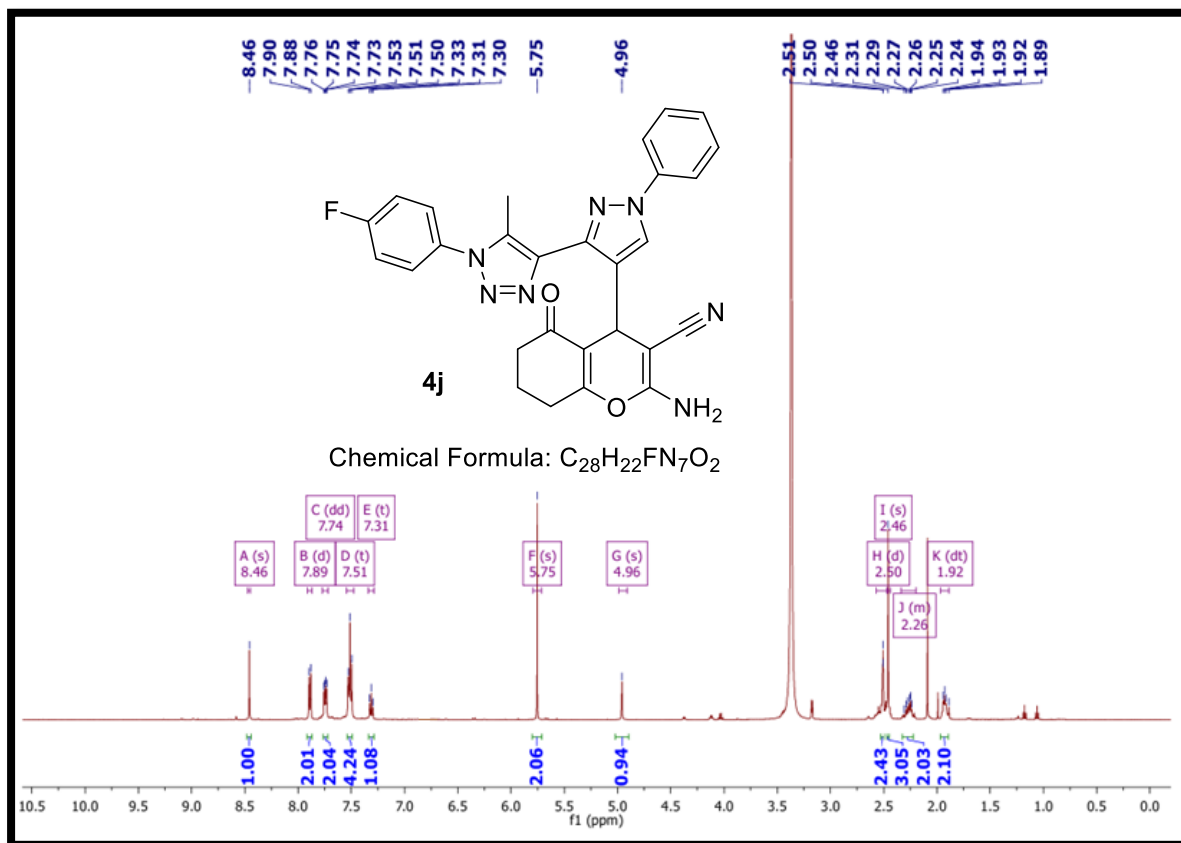
<sup>13</sup>C NMR of 2-amino-4-(3-(5-methyl-1-(p-tolyl)-1H-1,2,3-triazol-4-yl)-1-phenyl-1H-pyrazol-4-yl)-5-oxo-5,6,7,8-tetrahydro-4H-chromene-3-carbonitrile (4h)



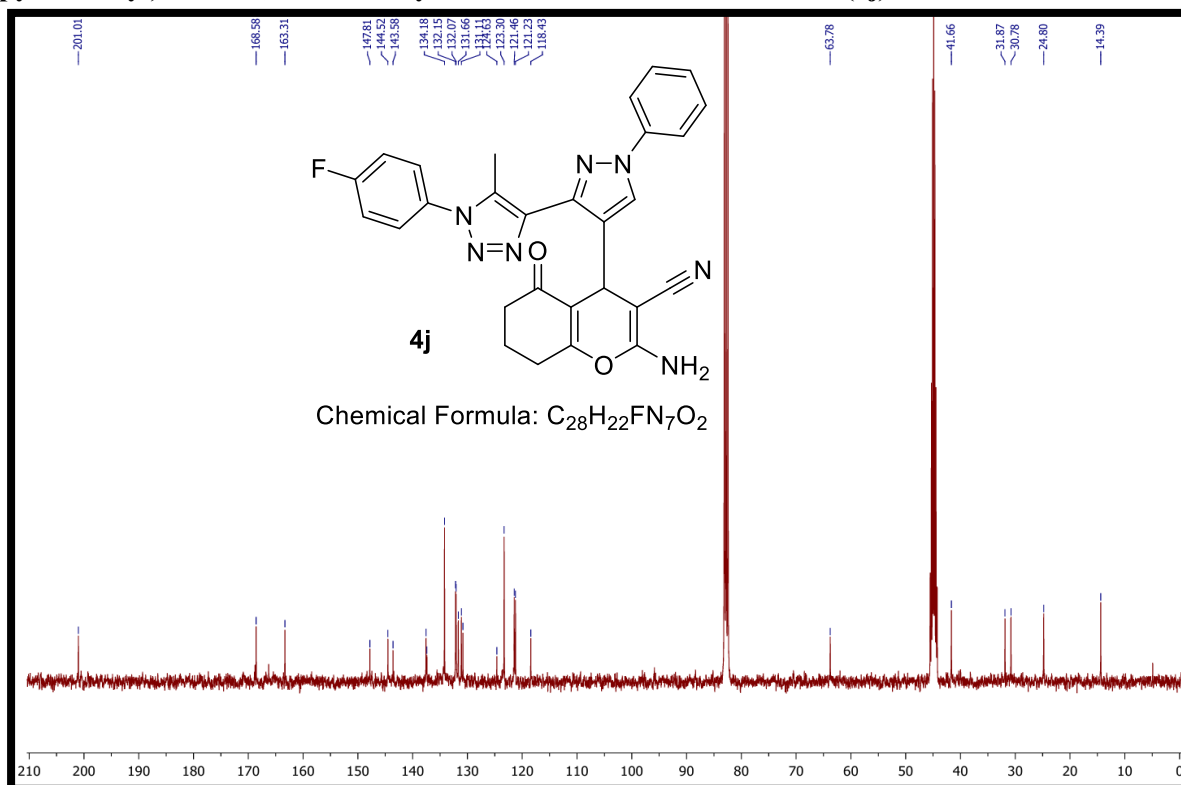
$^1H$  NMR of 2-amino-4-(3-(1-(4-chlorophenyl)-5-methyl-1H-1,2,3-triazol-4-yl)-1-phenyl-1H-pyrazol-4-yl)-5-oxo-5,6,7,8-tetrahydro-4H-chromene-3-carbonitrile (**4i**)



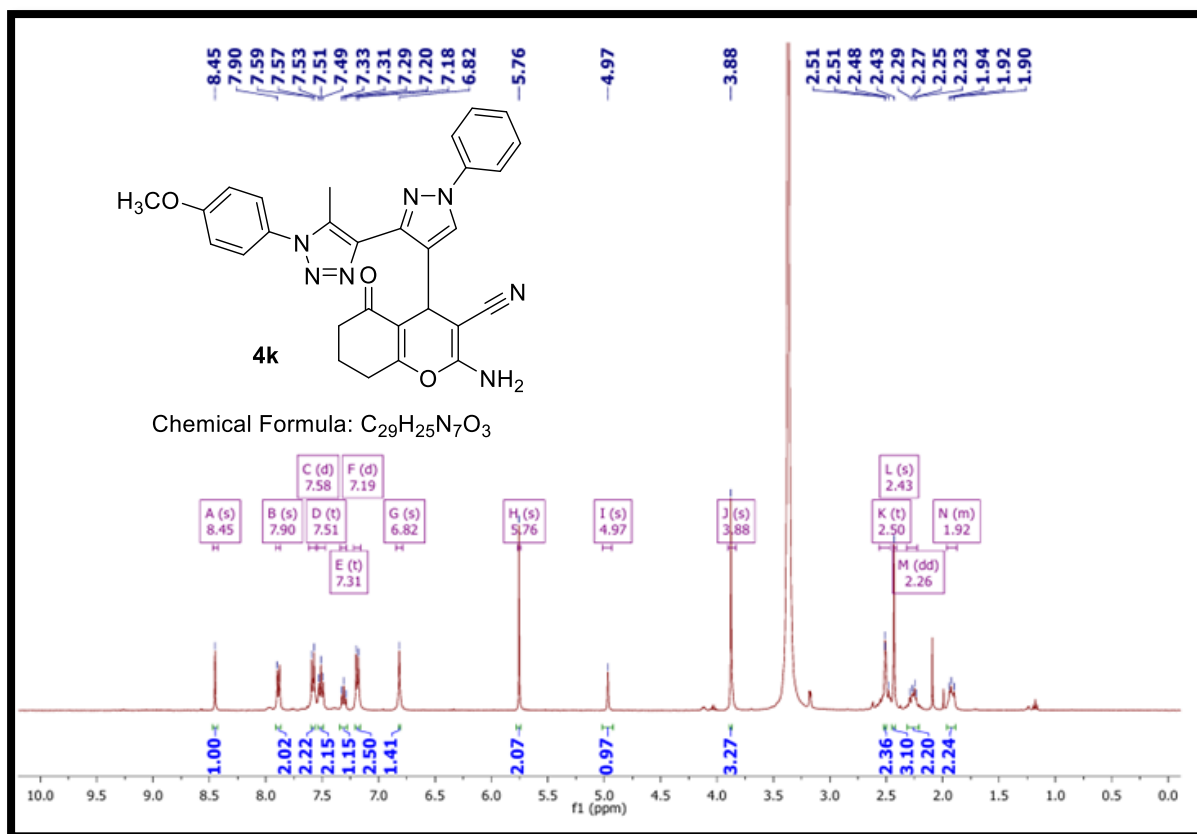
$^{13}C$  NMR of 2-amino-4-(3-(1-(4-chlorophenyl)-5-methyl-1H-1,2,3-triazol-4-yl)-1-phenyl-1H-pyrazol-4-yl)-5-oxo-5,6,7,8-tetrahydro-4H-chromene-3-carbonitrile (**4i**)



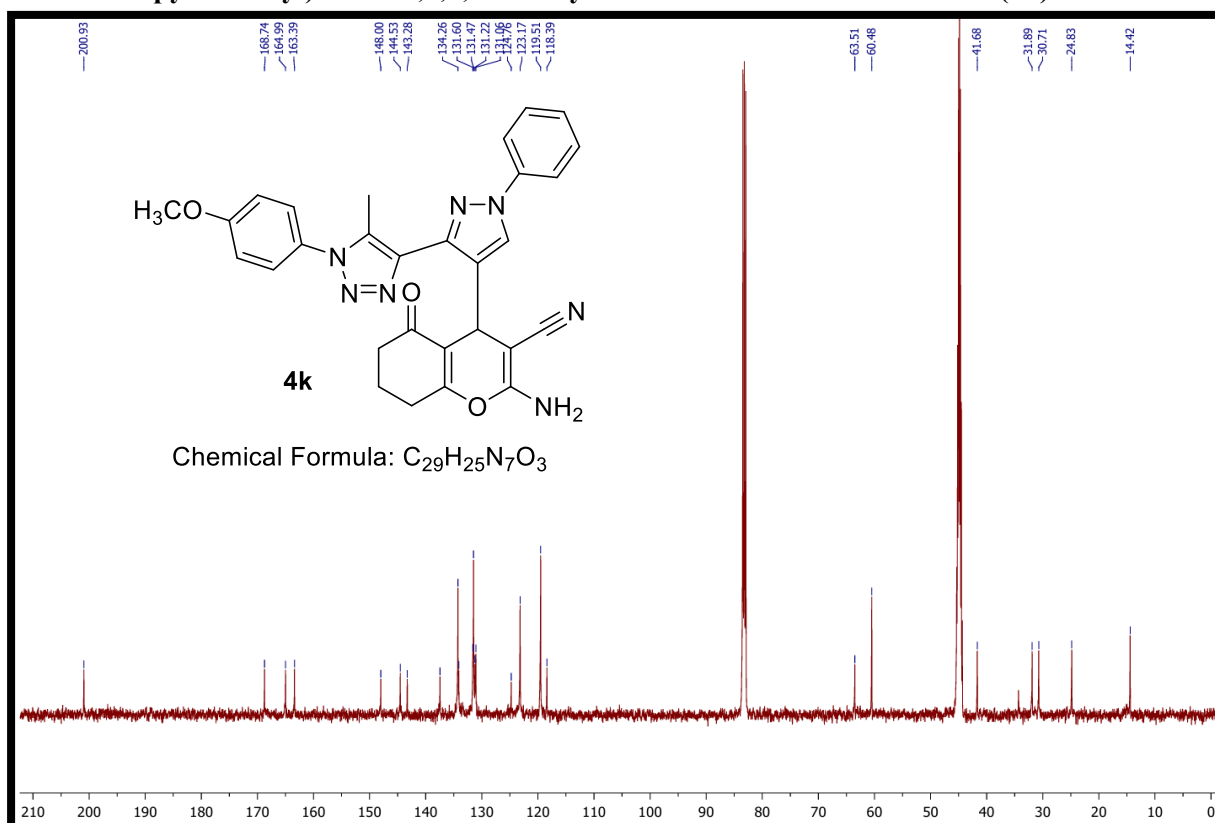
$^1H$  NMR of 2-amino-4-(3-(1-(4-fluorophenyl)-5-methyl-1H-1,2,3-triazol-4-yl)-1-phenyl-1H-pyrazol-3-yl)-5-oxo-5,6,7,8-tetrahydro-4H-chromene-3-carbonitrile (**4j**)



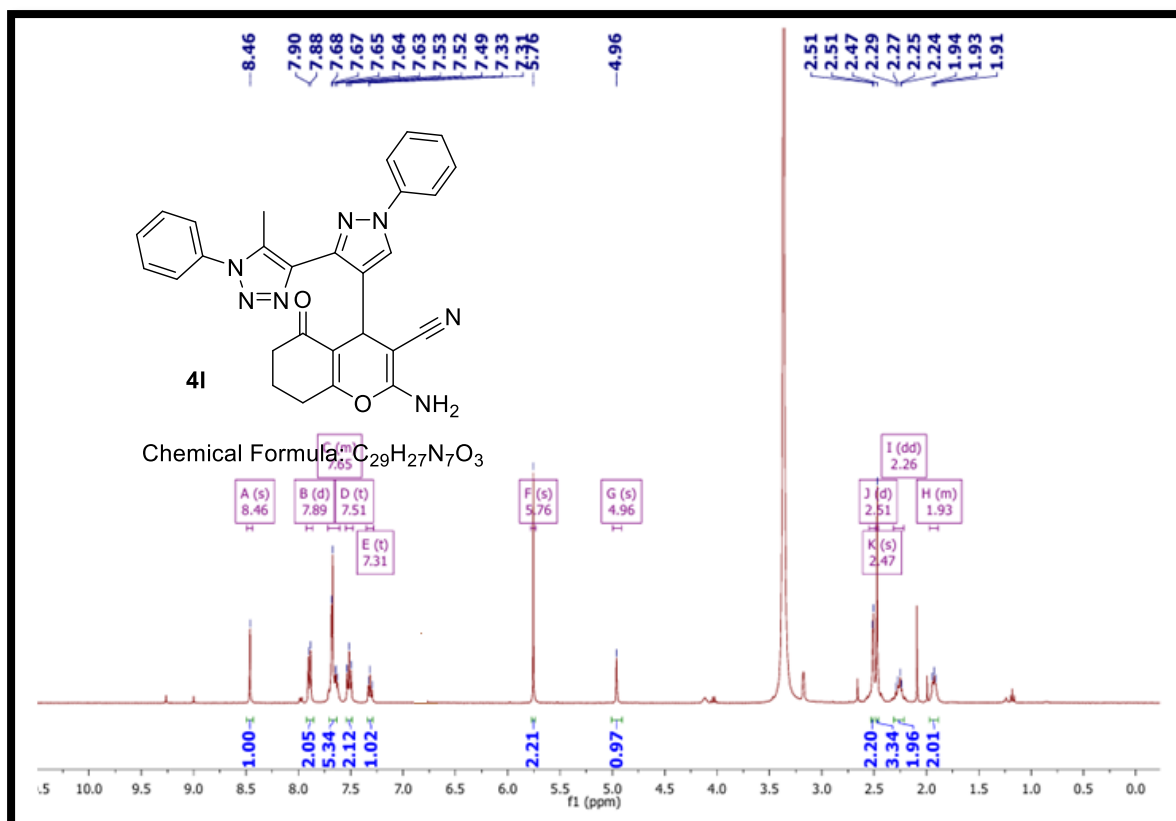
$^{13}C$  NMR of 2-amino-4-(3-(1-(4-fluorophenyl)-5-methyl-1H-1,2,3-triazol-4-yl)-1-phenyl-1H-pyrazol-3-yl)-5-oxo-5,6,7,8-tetrahydro-4H-chromene-3-carbonitrile (**4j**)



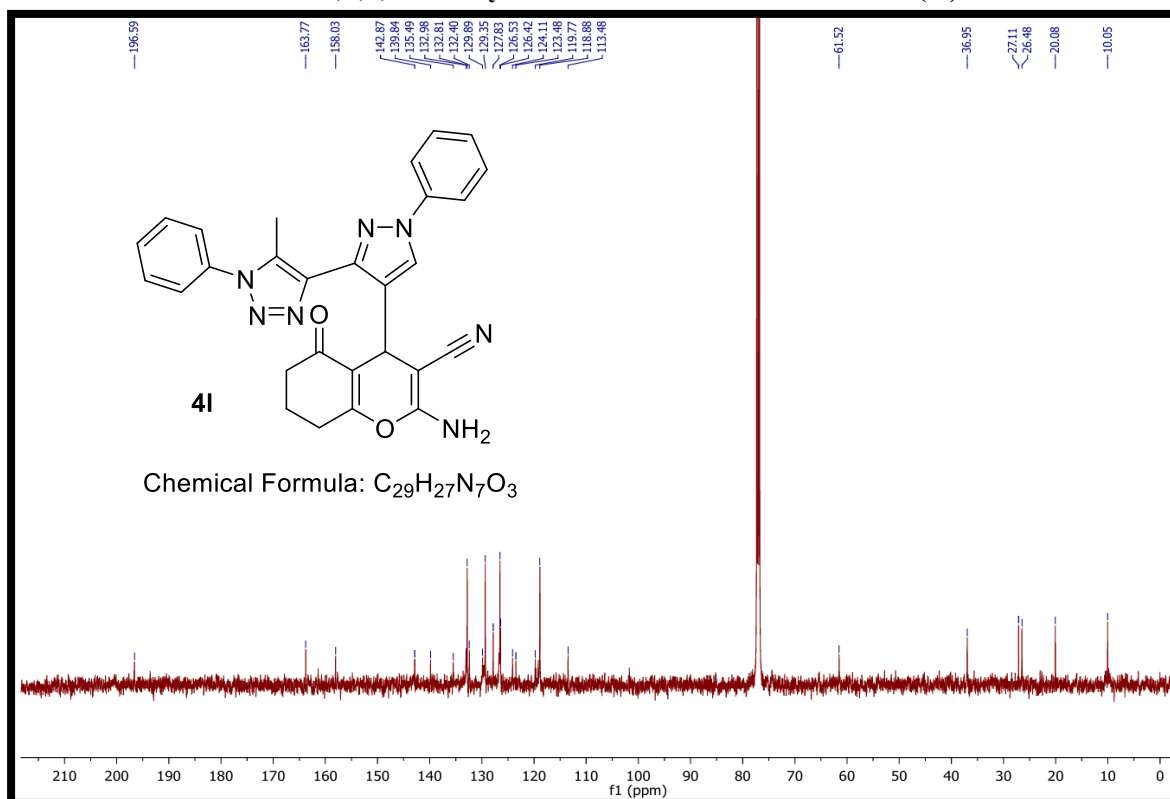
<sup>1</sup>H NMR of 2-amino-4-(3-(1-(4-methoxyphenyl)-5-methyl-1H-1,2,3-triazol-4-yl)-1-phenyl-1H-pyrazol-3-yl)-5-oxo-5,6,7,8-tetrahydro-4H-chromene-3-carbonitrile (4k)



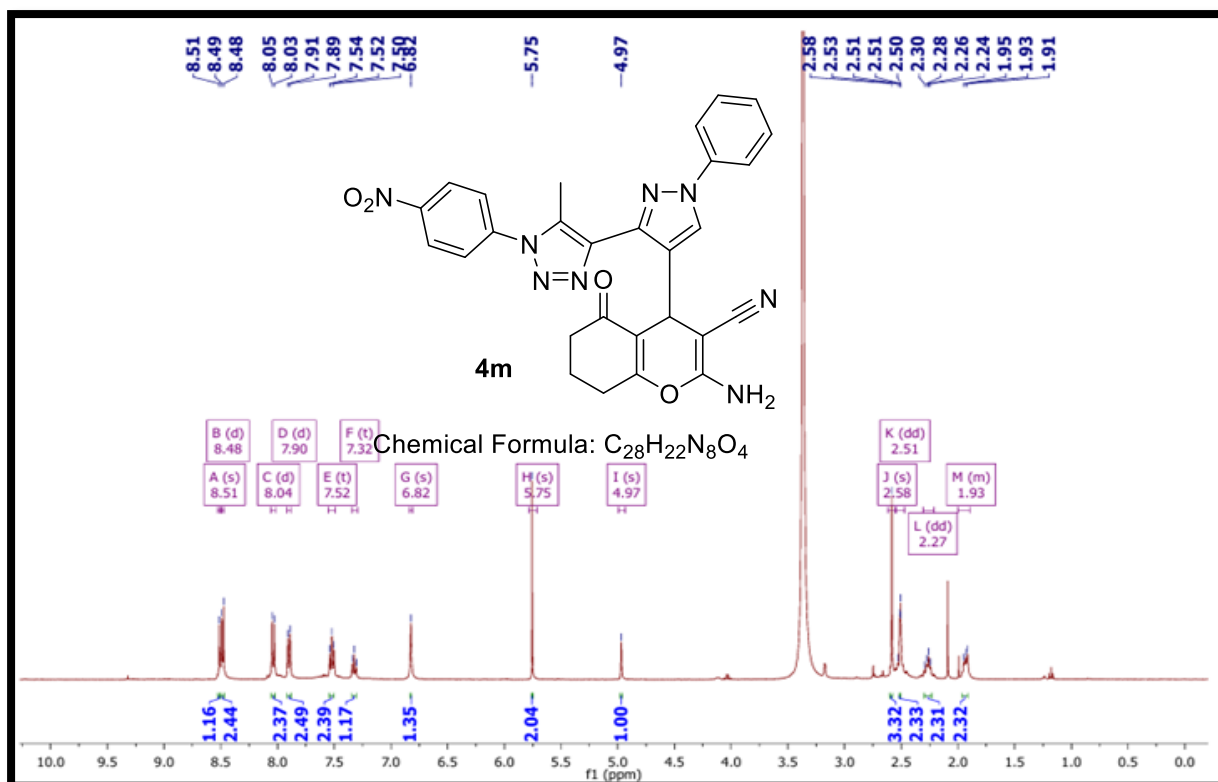
<sup>13</sup>C NMR of 2-amino-4-(3-(1-(4-methoxyphenyl)-5-methyl-1H-1,2,3-triazol-4-yl)-1-phenyl-1H-pyrazol-3-yl)-5-oxo-5,6,7,8-tetrahydro-4H-chromene-3-carbonitrile (4k)



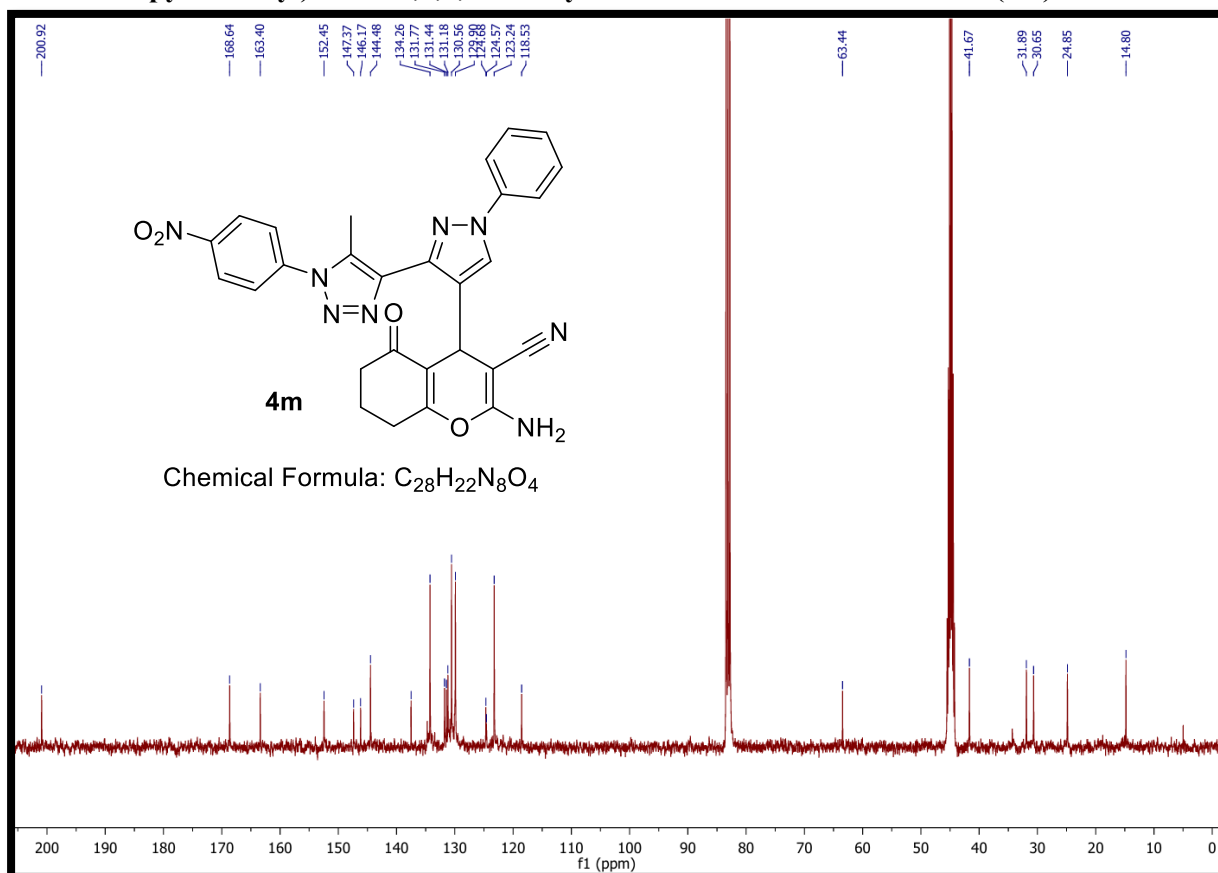
**$^1H$  NMR of 2-amino-4-(3-(5-methyl-1-phenyl-1H-1,2,3-triazol-4-yl)-1-phenyl-1H-pyrazol-3-yl)-5-oxo-5,6,7,8-tetrahydro-4H-chromene-3-carbonitrile (4l)**



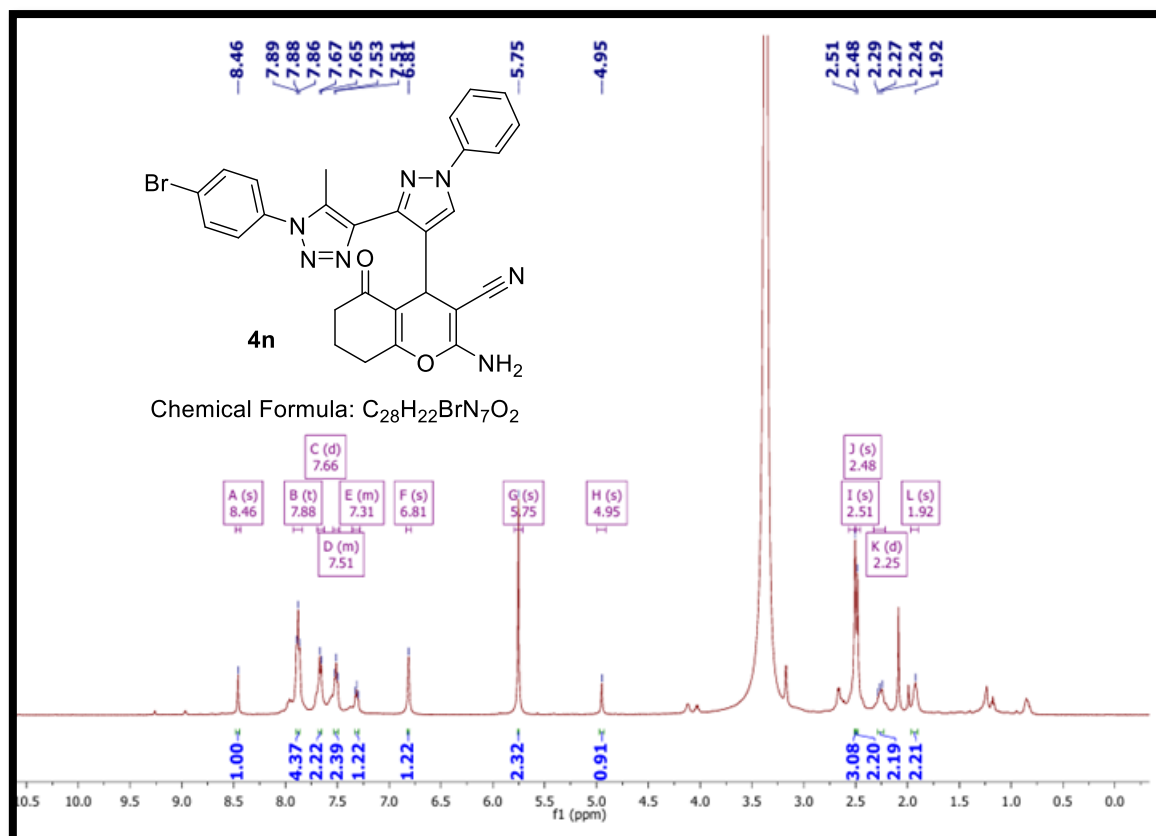
**$^{13}C$  NMR of 2-amino-4-(3-(5-methyl-1-phenyl-1H-1,2,3-triazol-4-yl)-1-phenyl-1H-pyrazol-3-yl)-5-oxo-5,6,7,8-tetrahydro-4H-chromene-3-carbonitrile (4l)**



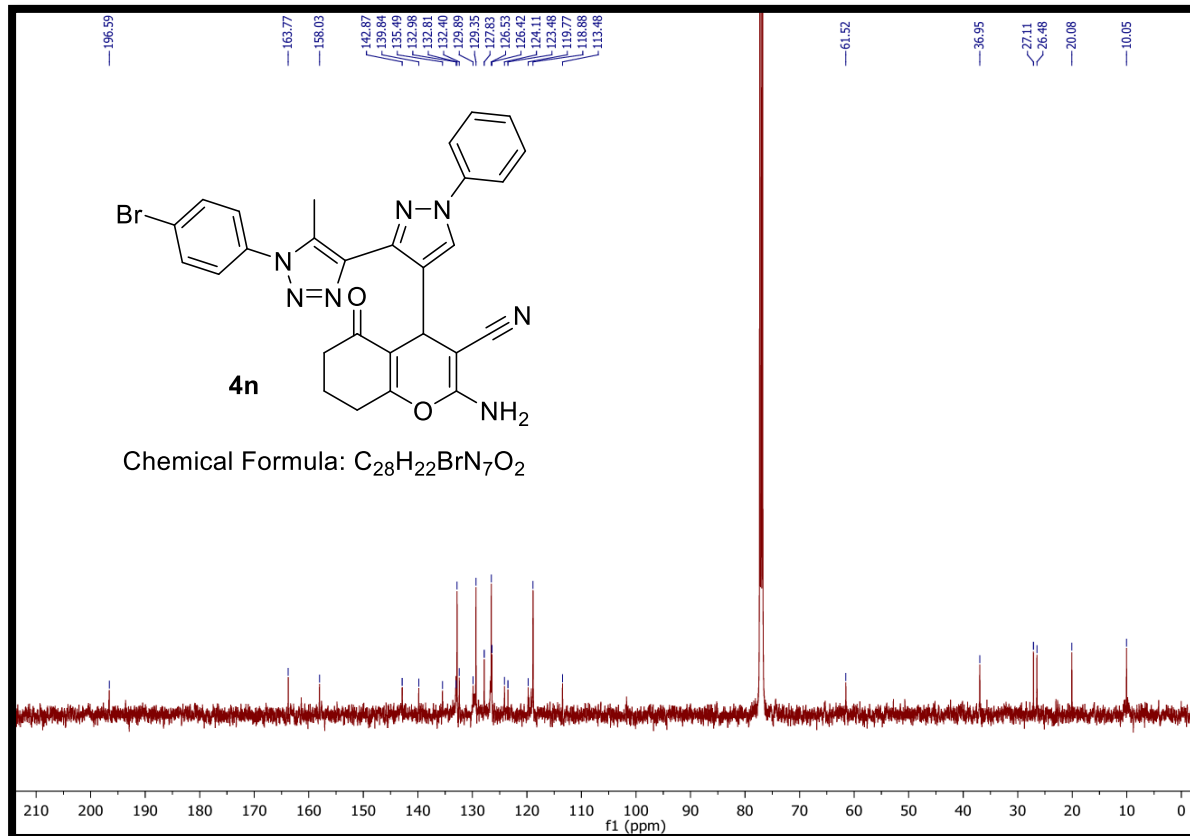
$^1H$  NMR of 2-amino-4-(3-(5-methyl-1-(4-nitrophenyl)-1H-1,2,3-triazol-4-yl)-1-phenyl-1H-pyrazol-3-yl)-5-oxo-5,6,7,8-tetrahydro-4H-chromene-3-carbonitrile (4m)



$^{13}C$  NMR of 2-amino-4-(3-(5-methyl-1-(4-nitrophenyl)-1H-1,2,3-triazol-4-yl)-1-phenyl-1H-pyrazol-3-yl)-5-oxo-5,6,7,8-tetrahydro-4H-chromene-3-carbonitrile (4m)



<sup>1</sup>H NMR of 2-amino-4-(3-(1-(4-bromophenyl)-5-methyl-1H-1,2,3-triazol-4-yl)-1-phenyl-1H-pyrazol-3-yl)-5-oxo-5,6,7,8-tetrahydro-4H-chromene-3-carbonitrile (4n)



<sup>13</sup>C NMR of 2-amino-4-(3-(1-(4-bromophenyl)-5-methyl-1H-1,2,3-triazol-4-yl)-1-phenyl-1H-pyrazol-3-yl)-5-oxo-5,6,7,8-tetrahydro-4H-chromene-3-carbonitrile (4n)

## References

1. Botta, M.; Armaroli, S.; Castagnolo, D.; Fontana, G.; Pera, P.; Bombardelli, E. *Bioorg Med. Chem. Lett.* **2007**, *17*, 1579.  
<https://doi.org/10.1016/j.bmcl.2006.12.101>
2. Mosmann, T. J. *Immunol. Methods* **1983**, *65*, 55.  
[https://doi.org/10.1016/0022-1759\(83\)90303-4](https://doi.org/10.1016/0022-1759(83)90303-4)
3. Acharya, R.; Chacko, S.; Bose, P.; Lapenna, A.; Pattanayak, S. P. *Sci. Rep.* **2019**, *9*, 15743.  
<https://doi.org/10.1038/s41598-019-52162-0>
4. Seshacharyulu, P.; Ponnusamy, M. P.; Haridas, D.; Jain, M.; Ganti, A. K.; Batra, S. K. *Expert Opin. Ther. Targets* **2012**, *16*, 15.  
<https://doi.org/10.1517/14728222.2011.648617>
5. Myakala, N.; Kandula, K.; Rayala, N.; Kuna, S.; Thumma, V.; Durga Bhavani Anagani, K. *Chem. Biodivers.* **2023**, *20*, e202300800.  
<https://doi.org/10.1002/cbdv.202300800>
6. Rejinthala, S.; Endoori, S.; Thumma, V.; Mondal, T. *Chem. Biodivers.* **2024**, *21*, e202301456.  
<https://doi.org/10.1002/cbdv.202301456>
7. Bax, B. D.; Chan, P. F.; Eggleston, D. S.; Fosberry, A.; Gentry, D. R.; Gorrec, F.; Giordano, I.; Hann, M. M.; Hennessy, A.; Hibbs, M.; Huang, J.; Jones, E.; Jones, J.; Brown, K. K.; Lewis, C. J.; May, E. W.; Saunders, M. R.; Singh, O.; Spitzfaden, C. E.; Shen, C.; Shillings, A.; Theobald, A. J.; Wohlkonig, A.; Pearson, N. D.; Gwynn, M. N. *Nature* **2010**, *466*, 935.  
<https://doi.org/10.1038/nature09197>
8. Sagatova, A. A.; Keniya, M. V.; Wilson, R. K.; Monk, B. C.; Tyndall, J. D. A. *Antimicrob. Agents Chemother.* **2015**, *59*, 4982.  
<https://doi.org/10.1128/AAC.00925-15>